

University of Windsor

## Scholarship at UWindor

---

Electronic Theses and Dissertations

Theses, Dissertations, and Major Papers

---

7-7-2020

# Factors Affecting Photovoltaic System Output in a Sub-Arctic Climate

Avinash Guya Singh  
*University of Windsor*

Follow this and additional works at: <https://scholar.uwindsor.ca/etd>

---

### Recommended Citation

Singh, Avinash Guya, "Factors Affecting Photovoltaic System Output in a Sub-Arctic Climate" (2020).  
*Electronic Theses and Dissertations*. 8398.  
<https://scholar.uwindsor.ca/etd/8398>

This online database contains the full-text of PhD dissertations and Masters' theses of University of Windsor students from 1954 forward. These documents are made available for personal study and research purposes only, in accordance with the Canadian Copyright Act and the Creative Commons license—CC BY-NC-ND (Attribution, Non-Commercial, No Derivative Works). Under this license, works must always be attributed to the copyright holder (original author), cannot be used for any commercial purposes, and may not be altered. Any other use would require the permission of the copyright holder. Students may inquire about withdrawing their dissertation and/or thesis from this database. For additional inquiries, please contact the repository administrator via email ([scholarship@uwindsor.ca](mailto:scholarship@uwindsor.ca)) or by telephone at 519-253-3000ext. 3208.

# **Factors Affecting Photovoltaic System Output in a Sub-Arctic Climate**

By

**Avinash G. Singh**

A Thesis

Submitted to the Faculty of Graduate Studies  
through the Department of Mechanical, Automotive and Materials Engineering  
in Partial Fulfilment of the Requirements for  
the Degree of Master of Applied Science at the  
University of Windsor

Windsor, Ontario, Canada

2020

© 2020 Avinash G. Singh

# **Factors Affecting Photovoltaic System Output in a Sub-Arctic Climate**

By

**Avinash G. Singh**

APPROVED BY:

---

R. Carriveau  
Department of Civil and Environmental Engineering

---

B-A. Schuelke-Leech  
Department of Mechanical, Automotive & Materials Engineering

---

P. Henshaw, Co-Advisor  
Department of Civil and Environmental Engineering

---

D. S-K. Ting, Co-Advisor  
Department of Mechanical, Automotive & Materials Engineering

April 30, 2020

## DECLARATION OF CO-AUTHORSHIP/PREVIOUS PUBLICATIONS

I hereby declare that this thesis incorporates material that is the result of joint research, as follows:

<b>Thesis Chapter</b>	<b>Details</b>
Chapter 2	This thesis also incorporates the outcome of a joint research undertaken under the supervision of Dr. Paul Henshaw, and Dr. David S-K. Ting. In all cases, the key ideas, primary contributions, data analysis and interpretation, were performed by the author, and the contribution of the co-author was primarily through the provision of supervision.
Chapter 3	This thesis also incorporates the outcome of a joint research undertaken under the supervision of Dr. Paul Henshaw, and Dr. David S-K. Ting. In all cases, the key ideas, primary contributions, data analysis and interpretation, were performed by the author, and the contribution of the co-author was primarily through the provision of supervision.

I am aware of the University of Windsor Senate Policy on Authorship and I certify that I have properly acknowledged the contribution of other researchers to my thesis, and have obtained written permission from each of the co-author(s) to include the above material(s) in my thesis.

I certify that, with the above qualification, this thesis, and the research to which it refers, is the product of my own work.

This thesis includes an original paper that has been previously submitted for publication in peer-reviewed journals, as follows:

<b>Thesis Chapter</b>	<b>Publication</b>	<b>Publication Status</b>
Chapter 2	Avinash Singh, Paul Henshaw, and David S.K. Ting, "Effect of Ambient Temperature and Wind On Solar PV Efficiency in A Cold Arctic Climate".	Submitted to International Journal of Environmental Studies on October 17, 2019.

<b>Thesis Chapter</b>	<b>Publication</b>	<b>Publication Status</b>
Chapter 3	Avinash Singh, Paul Henshaw, and David S.K. Ting, "Predicting the Horizontal Solar Irradiance (G) from Measured PV Output Power in Sub-Arctic Climate".	In preparation

I certify that I have obtained a written permission from the copyright owner(s) to include the above submitted material(s) in my thesis. I certify that the above material describes work completed during my registration as a graduate student at the University of Windsor.

I certify that, to the best of my knowledge, my thesis does not infringe upon anyone's copyright nor violate any proprietary rights and that any ideas, techniques, quotations, or any other material from the work of other people included in my thesis, published or otherwise, are fully acknowledged in accordance with the standard referencing practices.

I declare that this is a true copy of my thesis, including any final revisions, as approved by my thesis committee and the Graduate Studies office, and that this thesis has not been submitted for a higher degree to any other University or Institution.

## ABSTRACT

Photovoltaic arrays in the Arctic have been observed to produce power at values higher than their rated capacity. A solar photovoltaic (PV) array's efficiency depends on the PV cell temperature, which is based on the balance between solar isolation and heat loss. Two PV arrays in Iqaluit, Nunavut, Canada were studied to estimate the possible effects of panel cooling and albedo on the array efficiency. PV power (W) output data from the inverter and ambient temperature and wind speed data from Environment Canada from 2017 were used to estimate the effect of ambient temperature and wind speed on the solar PV array efficiency. These data were then used to estimate the horizontal solar irradiance ( $G$ ) at the locations in Iqaluit.

The first array has a PV panel reference efficiency of 15.89%, but performed at efficiencies of 16.1% to 18.8%. The efficiencies for the second array on the same days were 16.4% to 19.1% versus the PV panel reference efficiency of 16.16%. Considering an energy-weighted average of the efficiency enhancements for one clear and sunny day in each month, designers can expect the mean annual power output to be 4% to 7% above the rated output.

On selected clear and sunny winter, spring and summer days, during the period when both arrays were not affected by shading, the average difference in back calculated  $G$  between the arrays was 6 W/m<sup>2</sup> on the winter day while for the spring and summer day it was 6 W/m<sup>2</sup> and 28 W/m<sup>2</sup>. For the spring and summer, these represents deviations of 1% and 5%, respectively.

## DEDICATION

To my wife, children, parents, in-laws and friends.

## ACKNOWLEDGEMENTS

Several distinguished personalities have contributed in one way or another to making this thesis a reality.

I would like to express my sincere appreciation for the guidance, patience, and wisdom provided by my co-advisors, Dr. Paul Henshaw, and Dr. David S-K Ting. The guidance and support that they have provided to me from the start to the end of my program at the University of Windsor have been tremendous and essential in my development and completion of my studies. It was a great honor working with them in a fantastic Turbulence and Energy Laboratory, and have found both of them very polite, knowledgeable and accommodating whenever I have required their input. In addition, I must also give many thanks to the other committee members, Dr. Rupp Carriveau, and Dr. Beth-Anne Schuelke-Leech, for offering their tremendous knowledge on my research. In addition, I would like to acknowledge the assistance provided by Rong Luo from the Data Center in Leddy Library in helping me with plotting of graphs in Chapter 2 and Green Sun Rising Incorporated of Windsor, Ontario for providing me with the necessary PV data for the arrays in Iqaluit, Nunavut, Canada.

## TABLE OF CONTENTS

DECLARATION OF CO-AUTHORSHIP/PREVIOUS PUBLICATIONS .....	iii
ABSTRACT .....	v
DEDICATION .....	vi
ACKNOWLEDGEMENTS .....	vii
LIST OF TABLES .....	x
LIST OF FIGURES .....	xi
LIST OF APPENDICES .....	xiii
LIST OF ABBREVIATIONS/SYMBOLS .....	xiv
NOMENCLATURE .....	xvi
CHAPTER 1 INTRODUCTION .....	1
1.1 Background and Motivation .....	1
1.2 Objectives .....	5
REFERENCES .....	7
CHAPTER 2 EFFECT OF AMBIENT TEMPERATURE AND WIND ON SOLAR PV EFFICIENCY IN A COLD ARCTIC CLIMATE .....	11
2.1 Introduction .....	11
2.2 Solar PV Performance in Cold and Warm Temperatures .....	12
2.3 Solar PV Panel Efficiency .....	13
2.4 Solar PV Cell Temperature ( $T_c$ ) .....	14
2.4.1 Heat Loss from the Solar PV Arrays .....	15
2.4.1.1 Radiation ( $Q_{rad.}$ ) .....	15
2.4.1.2 The View Factor (F) .....	16
2.4.1.3 Sky Temperature ( $T_s$ ) .....	17
2.4.2 Convection .....	17
2.4.3 Energy Balance .....	18
2.5 Methodology .....	18
2.5.1 PV Output Data .....	18

2.5.2 Weather Data .....	20
2.5.3 Estimation of PV Actual Output Efficiency.....	22
2.5.4 Sensitivity Analysis .....	24
2.6 Results and Discussion .....	25
2.6.1 Energy Balance .....	28
2.6.1.1 Base Case.....	28
2.6.1.2 Sensitivity .....	30
2.6.2 Mean Annual Average .....	34
2.7 Conclusion and Future Plans .....	36
REFERENCES .....	38
CHAPTER 3 PREDICTING THE HORIZONTAL SOLAR IRRADIANCE (G) FROM MEASURED PV OUTPUT POWER IN SUB-ARCTIC CLIMATE.....	45
3.1 Introduction.....	45
3.2 Basic Solar Components .....	47
3.3 Methodology .....	50
3.3.1 PV Output Power Data.....	50
3.3.2 Estimation of Hourly Horizontal Solar Irradiance ( <i>G</i> ) .....	50
3.3 Calculation Procedure.....	52
3.4 Albedo Analysis.....	52
3.5 Comparison to Historical Values .....	52
3.6 Results and Discussions .....	54
3.7 Conclusion .....	61
REFERENCES .....	63
CHAPTER 4 CONCLUSIONS AND RECOMMENDATIONS.....	67
4.1 Summary and Conclusion .....	67
4.2 Recommendations.....	70
APPENDICES .....	71
REFERENCES .....	84
VITA AUCTORIS .....	85

## LIST OF TABLES

Table 1.1 Albedo values for various ground surfaces .....	4
Table 2.1 View factor for radiative heat loss from a PV array installed at a given tilt angle . .....	16
Table 2.2 PV Array Characteristics .....	20
Table 2.3. Estimated performance summary for both arrays.....	28
Table 2.4 1. Calculation of monthly energy-weighted relative efficiency enhancement at QEC (reference $\eta = 15.89\%$ ) .....	35
Table 2.5. Calculation of monthly energy-weighted relative efficiency enhancement at AWGA (reference $\eta = 16.16\%$ ).....	35
Table 3.1. Shows the average $G$ at no-shading versus shading and differences during the analysis for both arrays.....	58
Table 3.2 Shows the average $G$ and differences as the ground reflection varies for both arrays.....	60
Table 3.3 Shows the estimated values of $G$ compared to historic values and standard deviation .....	61
Table 1A Array Specifications.....	71

## LIST OF FIGURES

Figure 1.1 Power output of PV arrays in Sachs Harbour, Northwest Territories, Canada on April 24, 2016 .....	2
Figure 2. 1 Ambient temperature in Iqaluit for the days studied. ....	21
Figure 2. 2 Wind speed in Iqaluit for the day studied.....	22
Figure 2.3 Flow chart showing iterative calculation of $T_C$ and $\eta$ .. ....	24
Figure 2. 4 Reference and estimated PV efficiencies at QEC on January 1, 2017. ....	26
Figure 2. 5 Reference and estimated PV efficiencies at AWGA on January 1, 2017 .....	26
Figure 2. 6 Energy balance at QEC during the analysis period .....	29
Figure 2. 7 Energy balance at AWGA during the analysis period.....	30
Figure 2. 8 Mean change in h, $\Delta T$ and RDT at QEC for analysis period. ....	30
Figure 2.9 Energy balance error at QEC and AWGA for the analysis period (Swinbank sky temperature model and three convective heat transfer models).....	32
Figure 2.10 Energy balance error at QEC and AWGA for the analysis period (Bliss sky temperature model and three convective heat transfer models) .....	33
Figure 2.11 Energy balance error at QEC and AWGA for the analysis period ( $F_{\text{top-sky}}=0.5$ , Swinbank sky temperature model and three convective heat transfer models).....	33
Figure 2.12 Energy balance error at QEC and AWGA for the analysis period ( $F_{\text{top-sky}}=0.5$ , Bliss sky temperature model and three convective heat transfer models) .....	34
Figure 2.13 Mean monthly relative efficiency enhancements for both arrays compared to literature projects.....	36
Figure 3.1 Flow chart showing calculating of horizontal solar irradiance $G$ .....	53
Figure 3.2 Estimated horizontal solar irradiance ( $G$ ) for both arrays on January 1, 2017.....	55
Figure 3.3 Estimated horizontal solar irradiance ( $G$ ) for both arrays on May 26, 2017.....	56
Figure 3.4 Estimated horizontal solar irradiance ( $G$ ) for both arrays on July 2, 2017 .....	56
Figure 3.5 Albedo impact during the analysis period at QEC and AWGA .....	59
FigureA1 Array at QEC (Letters and numbers represent shading points) .....	72

FigureA2 Array at AWGA (Letters and numbers represent shading points) .....	72
FigureB1 Sun path and array shading at QEC for January 1, 2017 .....	74
FigureB2 Sun path and array shading at QEC for May 26, 2017 .....	74
FigureB3 Sun path and array shading at QEC for July 2, 2017 .....	75
FigureB4 Sun path and top array shading at AWGA for January 1, 2017 .....	75
FigureB5 Sun path and bottom array shading at AWGA for January 1, 2017 .....	76
FigureB6 Sun path and top array shading at AWGA for May 26, 2017 .....	76
FigureB7 Sun path and bottom array shading at AWGA for May 26, 2017 .....	77
FigureB8 Sun path and top array shading at AWGA for July 2, 2017 .....	77
FigureB9 Sun path and bottom array shading at AWGA for July 2, 2017 .....	78
FigureC1 Estimated irradiance for January 1, 2017 .....	82
FigureC2 Estimated irradiance for May 26, 2017 .....	83
FigureC3 Estimated irradiance for July 2, 2017 .....	83

## LIST OF APPENDICES

APPENDIX A: SOLAR PV ARRAYS AND SPECIFICATIONS .....	71
APPENDIX B: SUN PATH AND SHADING ANALYSIS .....	73
APPENDIX C: ESTIMATING THE HORIZONTAL SOLAR IRRADIANCE ( <i>G</i> ) USING A SIMULTANEOUS SOLUTION METHOD .....	79

## LIST OF ABBREVIATIONS/SYMBOLS

A	Area
AWGA	Arctic Winter Game Arena
$\beta$	Array Tilt Angle
Conv.	Convection
Cos	Cosine
Eff.	Efficiency
F	View Factor
G	Horizontal Solar Irradiance
$G_b$	Beam Irradiance on a Horizontal Surface
$G_d$	Diffuse Horizontal Irradiance
$G_o$	Extraterrestrial Horizontal Irradiation
$G_{on}$	Extraterrestrial Radiation
$G_t$	Solar Irradiance on the Tilted Array
h	Heat Loss Coefficient
I	Hourly Irradiation
$I_o$	Hourly Extraterrestrial Horizontal Irradiation
K	Kelvin
kJ	Kilojoules
Km	Kilometer
$k_T$	Sky Clearness Index
kW	Kilowatt
L	Latitude
m	Meter
NOCT	Nominal Operating Cell Temperature
P	Power
PV	Photovoltaic

$Q_{\text{rad}}$	Radiation Heat Loss
$Q_{\text{conv}}$	Convection Heat Loss
QEC	Qulliq Energy Corporation
Rad.	Radiation
$R_b$	Beam Radiation Tilt Factor
REE	Relative Enhance Efficiency
$REE_{\text{ewa}}$	Energy Weighted Average
Sin	Sine
STC	Standard Test Condition
T	Temperature
$T_a$	Ambient Temperature
$T_{a, \text{NOCT}}$	Nominal Operating Cell Temperature at Ambient Temperature
$T_c$	PV Cell Temperature
$T_{\text{dp}}$	Dew Point Temperature
$T_s$	Sky Temperature
$U_L$	Overall Heat Transfer Coefficient
$U_{L, \text{NOCT}}$	Overall Heat Transfer Coefficient at NOCT.
$V_w$	Wind Velocity
W	Watt
Z	Zenith

## NOMENCLATURE

$\alpha$	Absorptance
$\rho_g$	Albedo
$a_o$	Atmospheric Constant
$a_l$	Atmospheric Constant
$k$	Atmospheric Constant
$\tau_b$	Atmospheric Transmittance Coefficient from the Beam Radiation
$\tau_d$	Atmospheric Transmittance Coefficient from the Diffuse Radiation
$\eta$	Efficiency
$\varepsilon$	Emissivity
$A$	Geographic Altitude (Elevation)
$\tau$	Glazing
$\beta$	PV Cell Temperature Coefficient
$\sigma$	Stefan-Boltzmann Constant
$\gamma$	Solar Irradiance Coefficient
$\theta$	Solar Incident Angle
$\theta_Z$	Solar Zenith Angle
$\theta_\gamma$	Solar Azimuth Angle
$\omega$	Solar Hour Angle
$\delta$	Solar Declination Angle

## CHAPTER 1

### INTRODUCTION

#### **1.1 Background and Motivation**

The constant global rise of environmental challenges, increase in energy demand globally, and reduction in the availability of conventional energy resources such as fossil fuels have created a significant appetite for the use of renewable energy resources in meeting global energy consumption [1]. Renewable energy resources include solar, hydropower, biomass, wind and geothermal [2-3]. One of the most promising renewable energy resources in generating electricity is solar photovoltaic (PV), which converts the energy from sunlight into electricity without emitting any greenhouse gases. Thus, within the last decade, solar PV technology has shown tremendous growth globally [4-5] due to desires for energy independence, sustainability policies and strategies by governments in various countries, electrical efficiency improvement, and reduction in the unit cost for PV panels [6-10]. In addition, solar PV arrays are considered to be more economical for communities where the cost associated with using fossil fuels is very high [11]. Hence, many of Canada's northern communities fit perfectly into this category, since these communities are not connected to provincial electrical grids and receive almost all of their electrical energy from diesel generators using shipped-in fuel. Photovoltaic arrays installed in remote northern communities in Canada often generate power above their rated electrical output. Figure 1 below shows the output of a 15 kW PV array installed in a remote northern community [12].

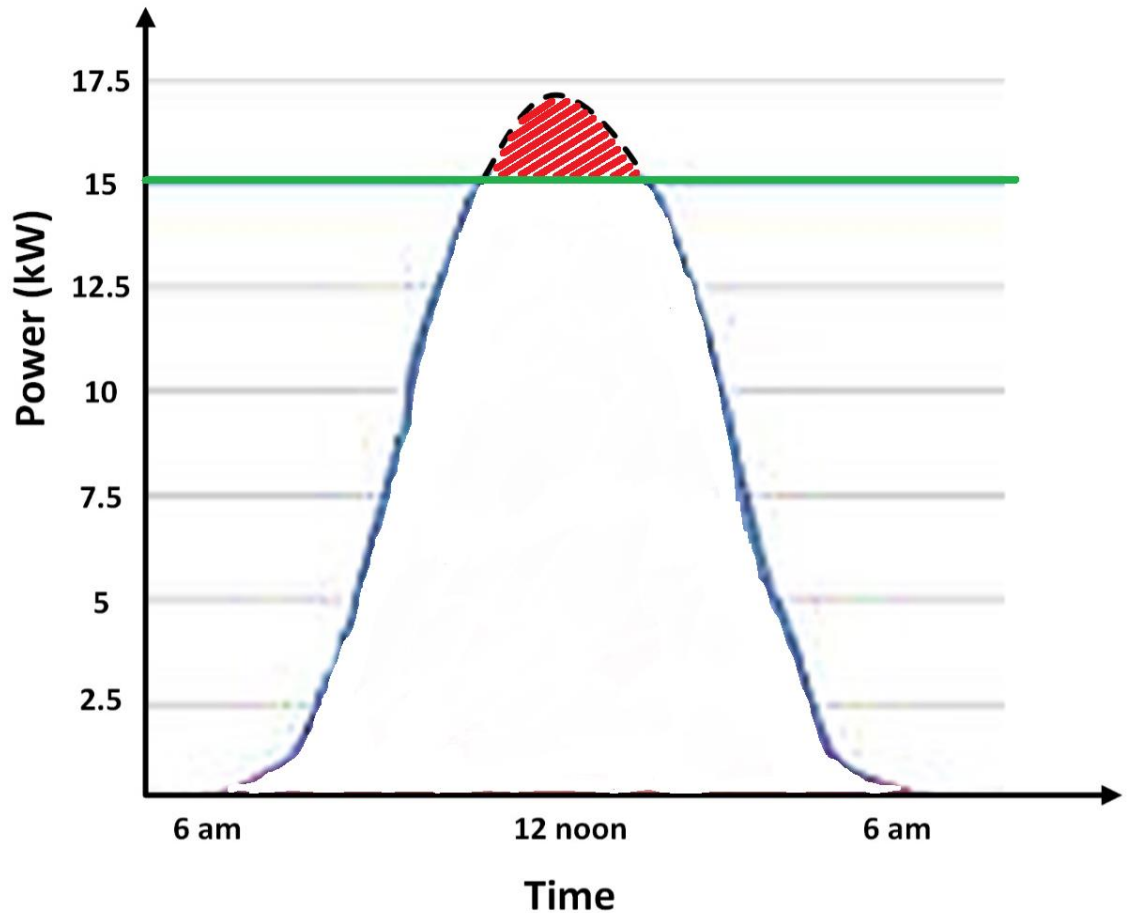


**Figure 1.1 Power output of PV arrays in Sachs Harbour, Northwest Territories, Canada on April 24, 2016 [adapted from Green Sun Rising Inc.]**

The inverter was sized based on the nominal output of the PV panels. Hence, the extra power generated by the array around noon is wasted, that is, the inverter is unable to convert all the power. There are three possible reasons for the PV panels to produce at above-rated quantities:

1. Low panel temperature

Solar PV panels are more efficient in colder climates than in warmer climates [13]. Solar PV cells have a negative temperature coefficient, that is, they have a greater efficiency at lower temperatures, thus an increase in the power [W] output

at a given light intensity. In warmer climates, there is a decrease in the efficiency, resulting in a decrease in the power [W] output [13].

Previous studies indicate that PV technology performs better in regions that are cold [15-21]. Pantic et al. [22] investigated solar PV performance in Serbia (southeastern Europe) during a typical winter and summer period to determine the actual PV output efficiency. During the winter period, the PV array had an enhanced efficiency and the power output was found to be greater than its rated capacity by approximately 16%, while during the summer it was found to perform at less than rated efficiency by approximately 10% [22]. Mondol et al. [23] looked at a 13 kW PV array installed on a roof in Northern Ireland and found the PV cell output and relative efficiency to be approximately ten percent (10%) less than rated during the summer season [23]. Another study reported on a 5.3 kW PV array installed on the East Coast of Saudi Arabia where the air temperature reached 60°C and the resulting output and relative electrical efficiency were 35 percent less than rated [24-25].

## 2. High surface albedo

Albedo is the fraction of radiation that reflects off a surface and is a factor in the ground reflection of radiation for the sun reflected by the earth surface. Table 1.1 shows albedo of different surfaces [13-14]

**Table 1.1 Albedo values for various ground surfaces [13-14]**

<b>Ground surface type</b>	<b>Albedo</b>
Fresh snow	0.7-0.9
Aged snow	0.6-0.8
Light-coloured paint	0.5-0.7
Ice	0.4-0.5
Melting snow	0.3-0.4
Grass	0.2-0.3
Sand	0.1-0.4
Soil	0.1-0.4
Concrete	0.1-0.3
Asphalt	0.1-0.2
Green forest	Less than 0.1

The surface albedo has an impact on the output of solar PV panels, especially in climates where the ground is covered by ice or snow. In some locations, the surface albedo could result in a reflected radiation of up to 1000 W/m<sup>2</sup> [14]. This effectively increases the energy to the PV panel.

### 3. Poor quantification of solar irradiation

When designing solar PV arrays it is important to know the solar irradiance for the location. The horizontal solar irradiance ( $G$ ) provides the PV system designer with knowledge of the amount of solar energy striking the earth's surface, from which the designer is able to determine the best tilt and azimuth angle for the array in order to

harness maximum solar irradiance, hence, generating maximum output power (W) [13]. However, in remote northern Canadian climates the horizontal solar irradiance ( $G$ ) data are unmeasured due to the high cost of measuring instruments and hence must be estimated from satellite-measured cloud cover data. Poor quantification of the solar resource may lead to underestimating the actual solar irradiance [13].

## 1.2 Objectives

The objective of this thesis is to determine the reasons for higher-than-rated output for Arctic solar PV arrays. First, the effects of ambient temperature, and wind velocity in estimating the output of solar PV under real operating conditions will be studied. Then, the output from two arrays at different orientations will be used to predict the horizontal solar irradiance ( $G$ ) so that it may be compared with available irradiance data for the site.

The subsequent chapters of this thesis are summarized as follows:

### Chapter 2 (Effect of Ambient Temperature and Wind Velocity)

This chapter addresses the estimated enhanced electrical efficiencies for two arrays in Iqaluit, Nunavut, Canada for clear and sunny days in each month of the year 2017. This analysis quantifies the influence of ambient temperature and wind on cooling the PV arrays and increasing their efficiency.

### Chapter 3 (Predicting Horizontal Solar Irradiance from Measured PV Power Output)

This chapter addresses the possibility of predicting the horizontal solar irradiance ( $G$ ) from measured PV power output data for the two arrays in Iqaluit. These arrays have

different azimuths but the same tilt. The plane-of-array irradiance values calculated in Chapter 2 were used to determine the horizontal solar irradiance ( $G$ ) in Iqaluit by back-calculation. The effect of albedo in this calculation was examined.

#### Chapter 4 (Conclusion and Future Works)

This chapter addresses conclusions from Chapters 2 and 3 and makes mention of possible future works.

#### Appendix A

This appendix provides the solar PV arrays locations and specifications.

#### Appendix B

This appendix provides plots of the sun path on January 1, May 26 and July 2 in Iqaluit, Nunavut, Canada and arrays shading at QEC and AWGA from sunrise to sunset.

#### Appendix C

This appendix introduces an alternative method of estimating the horizontal solar irradiance ( $G$ ) by forming two simultaneous equations for the two arrays in Iqaluit. However, the results obtained are poor, thus the method used in Chapter 3 was preferred over this method.

## REFERENCES

- [1] T. Kamal, S. Z. Hassan, H. Li, S. Mumtaz, L. Khan, (2016), Energy management and control of grid-connected wind/fuel cell/battery Hybrid Renewable Energy System, International Conference on Intelligent Systems Engineering, ICISE 28 -2 (2016) 955-964.
- [2] S. Kalogirou, Solar Energy Engineering, in: Processes and Systems, Elsevier Inc., Burlington, MA, 2009.
- [3] L. Yang, X. Gao, F. Lv, X. Hui, L. Ma, X. Hou, Study on the local climatic effects of large photovoltaic solar farms in desert areas, Solar Energy 144 (2017) 244–253.
- [4] R. Singh, M. Sharma, C. Banerjee, C, Field analysis of three different Silicon-based technologies in composite climatic condition. Solar Energy 182 (2019) 102-116.
- [5] C. Brunet, O. Savadogo, P. Baptiste, M.A, Bouchard, Shedding some light on photovoltaic solar energy in Africa – A literature review, Renewable and Sustainable Energy Reviews 96 (2018) 325-342.
- [6] M. Bayrakci, Y. Choi, J.R.S Brownson, Temperature dependent power modeling of photovoltaics, Energy Procedia 57 (2014) 745–754.
- [7] M. Habibollahi, M. Ameri, S.H. Mansouri, Efficiency improvement of photovoltaic water pumping systems by means of water flow beneath photovoltaic cells surface, Journal of Solar Energy Engineering 137-4 (2015) 044501.

- [8] T. Ma, W. Gu, L. Shen, L. M. Li, An improved and comprehensive mathematical model for solar photovoltaic modules under real operating conditions, *Solar Energy* 184 (2019) 292–304.
- [9] J.C. Solano, M. C. Brito, E. Caamaño-Martín, Impact of fixed charges on the viability of self-consumption photovoltaics, *Energy Policy* 122 (2018) 322-331.
- [10] J. Al-Saqlawi, K. Madani, N. Mac Dowell, Techno-economic feasibility of grid-independent residential roof-top solar PV systems in Muscat, Oman. *Energy Conversion and Management* 178 (2018) 322-334.
- [11] J. M. Pearce, S.V. Obydenkova, Technical viability of mobile solar photovoltaic systems for indigenous nomadic communities in northern latitudes, *Renewable Energy* 89 (2016) 253–267.
- [12] Green Sun Rising, Inc. (Private solar designers and contractors, Windsor, O. (2017). Solar PV output data for QEC and AWGA.
- [13] M. Ross, Photovoltaics in cold climates, in: James & James, Science Publishers Ltd, 1999, pp. 16–20.
- [14] P. Ineichen, O. Guisan, R. Perez. Ground-reflected radiation and albedo, *Solar Energy* 44 (1990) 207-214.
- [15] W.Tian, Y. Wang, J. Ren, L. Zhu, Effect of urban climate on building integrated photovoltaics performance, *Energy Conversion and Management* 48 (2007) 1–7.
- [16] N. Bowman, S. Shaari, Photovoltaics in buildings: A case study for rural England and Malaysia, *Renewable Energy* 15 (2002) 558–561.

- [17] E. Skoplaki, A.G. Boudouvis, J.A. Palyvos, A simple correlation for the operating temperature of photovoltaic modules of arbitrary mounting, *Solar Energy Materials and Solar Cells* 92 (2008) 1393–1402.
- [18] P. Trinuruk, C. Sorapipatana, D. Chenvidhya, Estimating operating cell temperature of BIPV modules in Thailand, *Renewable Energy* 34 (2009) 2515–2523.
- [19] J.L. Balenzategui, M.C. Alonso García, Estimation of photovoltaic module yearly temperature and performance based on nominal operation cell temperature calculations, *Renewable Energy* 29 (2004) 1997–2010.
- [20] E. Skoplaki, J. A. Palyvos, On the temperature dependence of photovoltaic module electrical performance: A review of efficiency/power correlations, *Solar Energy* 83 (2009) 614–624.
- [21] E. Skoplaki, J. A. Palyvos, Operating temperature of photovoltaic modules: A survey of pertinent correlations, *Renewable Energy* 34 (2009) 23–29.
- [22] L.S. Pantic, T.M. Pavlović, D.D. Milosavljević, I.S. Radonjic, M.K. Radovic, G. Sazhko, The assessment of different models to predict solar module temperature, output power and efficiency for Nis, Serbia, *Energy* (2016) 38–48.
- [23] J.D. Mondol, Y. Yohanis, M. Smyth, B. Norton, Long term performance analysis of a grid connected photovoltaic system in Northern Ireland, *Energy Conversion and Management*, 47-18 (2006) 2925–2947.
- [24] A. Vasel, F. Iakovidis, The effect of wind direction on the performance of solar PV plants, *Energy Conversion and Management* 153 (2017) 455–461.

[25] I. El-Amin, S. Rehman, Performance evaluation of an off-grid photovoltaic system in Saudi Arabia, *Energy* 46-1 (2012) 451–458.

## CHAPTER 2

### EFFECT OF AMBIENT TEMPERATURE AND WIND ON SOLAR PV EFFICIENCY IN A COLD ARCTIC CLIMATE

#### **2.1 Introduction**

Renewable energy resources include solar, hydropower, biomass, wind and geothermal [1-2]. Solar photovoltaic (PV) installation and usage over the last decade has grown tremendously because of advantages such as reducing greenhouse gas emissions, energy independence and sustainability policies and strategies, and efficiency improvement and reduction in unit cost for (PV) panels [3-5]. In addition, solar PV is considered along with wind energy to be one of the cheapest sources of renewable energy when compared to fossil fuel in generating electric power in the present energy market [6]. The electrical efficiency of a solar PV panel/array is dependent on various environmental conditions such as ambient temperature, wind speed and albedo [7-8]. PV arrays can be economic for communities where the cost of getting fossil fuels is very expensive due to limited transportation options [9]. Many of the isolated communities located in Canadian northern territories fall into this category, as they receive almost all of their electrical energy from diesel generators. The dependence on fossil fuels results in electrical utilities with high operational and environmental costs. Increasing the use of renewable energy, such as PV technologies, supports energy sustainability and the region's future development [10].

PV technology has been perceived as a good performer in hot and dry climates due to the available solar energy throughout the year as compared with cold climates having shorter days during the winter season. However, PV technology performs better in

regions that are cold, due to the fact that the PV cells become cooler and thus more efficient [11-18].

This paper analyses the actual electrical efficiency performance of two separate solar PV arrays located in Iqaluit, Canada. Iqaluit is located close to the Arctic Circle, at a latitude of 63.75 degrees north, and is the capital of the territory of Nunavut [19]. Array efficiencies were estimated from array power output data measured by the inverters and manufacturers' reference efficiencies, modified by the effects of ambient temperature and wind. In addition, no on site measurement of solar irradiance and electrical power by strings were done or available. Further analysis was performed to understand the heat loss mechanisms at various times of the year. Sensitivity of the energy balance to the use of different equations describing the convective heat loss coefficient, sky temperature and view factors was examined. The annual mean relative enhancement in efficiency was calculated.

## **2.2 Solar PV Performance in Cold and Warm Temperatures**

The efficiency of a PV array increases and decreases linearly depending on the ambient temperature. Specifically, increasing the PV cell temperature will result in its output voltage significantly decreasing and its current slightly increasing; thus the overall impact is a decrease in the output power. As the ambient temperature increases, the array efficiency decreases, while as the ambient temperature decreases the array efficiency increases [20]. Pantic *et al.* investigated solar PV performance in Serbia (south-eastern part of Europe) during a typical winter and summer period to determine the actual PV output efficiency. During the winter period, the PV array efficiency was found to be greater than its rated capacity by approximately 16% while during the summer it was

found to perform at less than rated efficiency by approximately 10% [21]. In addition, in an experiment done by Kasaeian *et al.* [22] where a PV array was subjected to forced convection by cold air, the efficiency increased by approximately 12% above the rated efficiency [23]. Mondol *et al.* [24] looked at a 13 kW PV array installed on a roof in Northern Ireland and found the PV cell output to be approximately ten percent (10%) less than rated during the summer season when the temperature was warm [25]. Another study reported on a 5.3 kW PV array installed on the East Coast of Saudi Arabia where the air temperature reached to 60°C and the resulting output was 35 percent less than rated efficiency [25-26]. Thus, one would expect to see a significant increase in the solar PV efficiency for the solar PV arrays in Iqaluit where the ambient temperature is cold most of the year.

### 2.3 Solar PV Panel Efficiency

The solar PV panel efficiency is determined by dividing the electric DC power output by the input irradiance on the surface [27],

$$\eta = \frac{P}{AG_t} \quad (1)$$

where  $P$  is the power output (in W),  $A$  is the area of the array (in m<sup>2</sup>), and  $G_t$  is the solar irradiance on the tilted surface of the array (W/m<sup>2</sup>). However, the efficiency of the solar PV panel is influenced by the PV cell temperature and irradiance which can simply be estimated [27-28],

$$\eta = \eta_{ref} \left[ 1 - \beta(T_c - T_{ref.}) + \gamma \text{Log} \frac{G_t}{G_{ref}} \right] \quad (2)$$

where  $\eta_{ref}$  is the PV cell efficiency at standard reference conditions ( $G_{ref}$  is 1000 W/m<sup>2</sup> and  $T_{ref}$  is 298 K),  $\gamma$  and  $\beta$  are solar irradiance and temperature coefficients, respectively

- these values are normally provided by the PV panel manufacturers. The solar irradiance coefficient ( $\gamma$ ) is typically assumed to be zero, thus Equation 2 simplifies to Equation 3 [27-29].

$$\eta = \eta_{ref} [1 - \beta(T_C - T_{ref})] \quad (3)$$

#### 2.4 Solar PV Cell Temperature ( $T_c$ )

Typically, for every 1°C rise above  $T_{ref}$ , the PV panel cell efficiency decreases by 0.25% for amorphous cells whilst for crystalline cells it decreases 0.4-0.5% [30]. These values can directly be used as the temperature coefficient  $\beta$  (%/K), in Equation 3. The electrical efficiency and temperature coefficient of the solar PV panel are measured by PV manufacturers. Under Standard Reference Conditions (IEC 904-1 and IEC 60904-3) the solar PV panel is allowed to rest horizontally in the lab under electric lights, creating a simulated solar irradiance of 1000 W/m<sup>2</sup> on the PV cells with the ambient temperature set to a constant value (298 K for  $T_{ref}$ , others to determine  $\beta$ ), and its current and voltage output are measured [31, 32].

An estimate of the maximum PV cell temperature is measured during the Nominal Operating Cell Temperature (NOCT) test 3 [27, 31]. This test is done on an open-rack PV panel under an open circuit condition when the solar irradiance on the tilted surface is 800 W/m<sup>2</sup> with the PV panel tilted at 45° from the horizontal, at an ambient temperature of 293K and air velocity of 1 m/s parallel to the panel. The solar PV cell temperature can be estimated from Equation 4 [1, 27, 31, 33-34],

$$T_C = T_a + (T_{NOCT} - T_{a,NOCT}) \left( \frac{G_t}{G_{t,NOCT}} \right) \left( \frac{U_{L,NOCT}}{U_L} \right) \left( \frac{1-\eta}{\tau\alpha} \right) \quad (4)$$

where  $T_a$ ,  $T_{NOCT}$ ,  $T_{a,NOCT}$ ,  $G_{t,NOCT}$ ,  $U_L$ ,  $U_{L,NOCT}$ ,  $\tau$  and  $\alpha$  are ambient temperature (K), nominal operation cell temperature (K), ambient temperature during the NOCT test (293 K), solar irradiance during the NOCT test (800 W/m<sup>2</sup>), overall heat loss coefficient (W/m<sup>2</sup>·K), overall heat loss coefficient during the NOCT test (W/m<sup>2</sup>·K), transmittance of glazing, and absorptance of the PV cell, respectively

### 2.4.1 Heat Loss from the Solar PV Arrays

After neglecting the conduction from the PV modules to the mounting structure, the overall heat loss coefficient can be estimated [27],

$$U_L = \frac{Q_{rad}}{A(T_C - T_a)} + h \quad (5)$$

where  $Q_{rad}$  and  $h$  are the radiation heat loss (in W), and convection heat transfer coefficient (W/m<sup>2</sup>·K), respectively.

#### 2.4.1.1 Radiation ( $Q_{rad}$ )

According to Armstrong and Hurley, heat loss due to radiation from the PV arrays occurs from the PV top to the sky and the ambient air, and from the PV bottom to the ground, wall and ambient air, expressed as in Equation 6 [1, 27, 35-36].

$$Q_{rad} = Q_{rad,top} + Q_{rad,bottom} \quad (6)$$

In addition, it is assumed that the temperatures of the covers on the top and bottom of the PV module are equal to the module's cell temperature and that the ground and wall temperatures are equal the ambient temperature, thus radiation from both top and bottom can be estimated [1, 27, 35-37],

$$Q_{rad} = \varepsilon_1 \sigma F_1 A (T_C^4 - T_S^4) + \varepsilon_1 \sigma F_2 A (T_C^4 - T_{g/w}^4) + \varepsilon_2 \sigma F_3 A (T_C^4 - T_{g/w}^4) \quad (7)$$

where  $\varepsilon_1, \varepsilon_2, \sigma, F_1, F_2, F_3, T_s, T_g$  and  $T_w$  are emissivity of the solar PV module at the top and bottom (0.91 and 0.85 at the top and bottom, respectively) [25, 33], Stefan-Boltzmann constant ( $5.67 \times 10^{-08} \text{ W/m}^2 \cdot \text{K}^4$ ), view factors, sky temperature (K), ground temperature (K), and wall temperature (K), respectively.

### 2.4.1.2 The View Factor (F)

The view factor ( $F$ ) is the geometric fraction of the entire  $180^\circ$  that the solar PV array “sees” which is occupied by another body (sky, ground, or wall). Table 2.1 lists equations used to estimate the view factor from PV top to sky, PV top to ground and wall, and PV bottom to ground and wall, respectively [27, 36]. The view factor for PV bottom to ground and wall is the sum of Equations 10 and 11 in Table 2.1, resulting in a sum of 1 always. Hence,  $F_3 = 1$ . In the case of a façade-mounted PV array,  $90^\circ$  of the  $180^\circ$  view is occupied by the sky, so the alternative view factors could be used:  $F_1 = 0.5$ , and  $F_2 = 0.5$ .

**Table 2.1 View factor for radiative heat loss from a PV array installed at a given tilt angle [27, 36].**

View factors location	Expression
PV Top to Sky ( $F_1$ )	$\frac{1}{2}(1 + \cos\beta)$ (8)
PV Top to Ground and Wall ( $F_2$ )	$\frac{1}{2}(1 - \cos\beta)$ (9)
PV Bottom to Ground	$\frac{1}{2}[1 + \cos(180^\circ - \beta)]$ (10)
PV Bottom to Wall	$\frac{1}{2}[1 - \cos(180^\circ - \beta)]$ (11)

$\beta$  is the tilt angle of the array from horizontal.

### 2.4.1.3 Sky Temperature ( $T_s$ )

There are numerous models available for estimating the sky temperature. The Swinbank model provides the sky temperature using only the local ambient temperature as input. Thus, the sky temperature (K) can be estimated from Equation 12 [1, 27, 35, 38].

$$T_s = 0.0552T_a^{1.5} \quad (12)$$

Bliss developed an equation where the sky temperature is related to the water vapor content of the ambient air [39],

$$T_s = T_a \left[ 0.8 + \frac{T_{dp} - 273}{250} \right]^{0.25} \quad (13)$$

where  $T_{dp}$  is the dew point temperature (K).

### 2.4.2 Convection

According to Hurley and Armstrong (2010), the convective heat loss from the PV array occurs at its top and bottom surfaces with exchange taking place with the ambient air and can be characterized as [27, 35-36],

$$Q = Q_{conv,top} + Q_{conv,bottom} \quad (14)$$

$$Q_{conv,i} = h_i A (T_c - T_a) \quad (15)$$

where  $Q_{conv,top}$  and  $Q_{conv,bottom}$  are the convective heat losses from top and bottom of the PV arrays to the ambient air (W), respectively.

Three relationships between the convective heat loss coefficient,  $h$ , and the wind speed,  $V_w$  (m/s), are shown in Equations 16, 17, and 18 below. Test *et al.* [40] collected

their data outdoors using natural wind, and the wind speed was measured 1 m above the array.

$$h = 2.56V_w + 8.55 \quad (16)$$

Charlesworth & Sharples (1998) measured the wind speed windward of the array [41].

$$h = 3.3V_w + 6.5 \quad (17)$$

Sturrock & Cole (1977) measured the wind speed leeward of the array, blowing parallel to the long dimension of the array [42].

$$h = 5.7V_w \quad (18)$$

### 2.4.3 Energy Balance

At steady-state, the energy entering and leaving the PV array achieves equilibrium, that is the PV array receives energy from sunlight ( $G_t$ ) and there are losses of energy in the form of heat through radiation and convection, and in the form of electricity. The error in the energy balance is expressed [43],

$$\% \text{ Error} = 100[G_t A - \sum(Q_{rad} + Q_{conv} + P)]/(G_t A) \quad (19)$$

## 2.5 Methodology

### 2.5.1 PV Output Data

PV output power, ambient temperature and wind speed data were acquired for a 2.86 kW array installed at Qulliq Energy Corporation (QEC) and a 10.4 kW array at the Arctic Winter Games Arena (AWGA) for clear and sunny days in Winter (1<sup>st</sup> January), Spring (26<sup>th</sup> May) and Summer (2<sup>nd</sup> July), 2017. The data used for the analyses was for

the period 11:50 to 13:05 hours on January 1, while for May 26 and July 2 it was from 11:00 to 19:00 hours for both arrays. Although data are available throughout the day, there were significant power fluctuations under low solar altitude conditions, thus making it difficult to analyze. A threshold of 300 W was implemented, such that the time when the power (P) was greater than 300 W was considered in the analysis. For comparison, during the winter solstice, the average day in Iqaluit lasts approximately 4 ½ hours whilst at the summer solstice it is approximately 20 hours.

The PV output power (DC) data for both locations was obtained from Fronius IG plus 10 kW Inverters (Wels, Austria) which are remotely monitored by Green Sun Rising Incorporated (solar designers and contractors in Windsor, Ontario, Canada; personal communication), and the ambient temperature and wind speed data was obtained from Environment Canada [44]. Both ambient temperature and wind speed data were recorded at the Iqaluit International Airport, which is located approximately 2.6 km from QEC and 4.2 km from AWGA [45]. The wind speed was measured at a height of 10 m from the ground surface [46]. The arrays at both locations are façade-mounted with a tilt angle of 60° (solar designers and contractors in Windsor, Ontario, Canada; personal communication) and are located approximately 2 km apart from each other [46]. Table 2.2 summarizes the PV panels used in these arrays.

**Table 2.2 PV Array Characteristics [47-48]**

Location	Type of Modules	Array Area [m <sup>2</sup> ]	Number of Modules in Array	Azimuth [°]	Module NOCT [K]	Temperature Coefficient of Maximum Power, $\beta$ [%/ K]	Nominal Maximum Rated Power [W]	Panel Reference Efficiency, $\eta_R$ [%]
QEC	Jinko Solar JKM260pp-60 Poly-crystalline	18.0	11	45.0	318±2	0.42	260	15.89
AWGA	Canadian Solar CS6P-260 Poly-crystalline	64.3	40	11.3	318±2	0.41	260	16.16

### 2.5.2 Weather Data

Figure 2.1 shows the ambient temperature for January 1, May 26, and July 2, 2017 at hourly intervals. From the plot, it is observed that the coldest of the three days was January 1 when the temperature fluctuated between -17°C and -23°C, whilst on May 26 and July 2, the temperature fluctuated between -5°C and 5°C, and 7°C and 16°C, respectively [44]. However, during the analysis period the ambient temperatures ranged from -19°C to -21°C on the January 1, whilst on May 26 and July 2 the ranges were 3°C to 5°C and 14°C to 15°C, respectively.

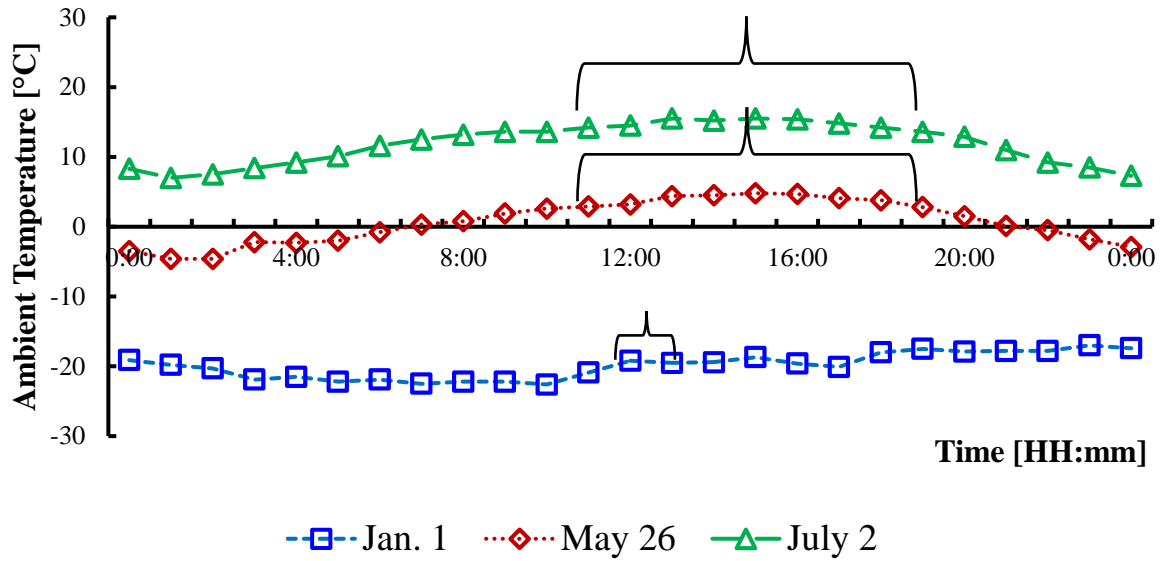


Figure 2. 1 Ambient temperature in Iqaluit for the days studied. The bracket shows the analysis period at QEC.

Figure 2.2 shows the wind speed data for January 1, May 26, and July 2 at hourly intervals. From the plot, it is observed that on January 1, the wind speed fluctuated from 4 m/s to 6 m/s, whilst for May 26 and July 2, it was fluctuating from 4 m/s to 7 m/s for the analysis period [44].

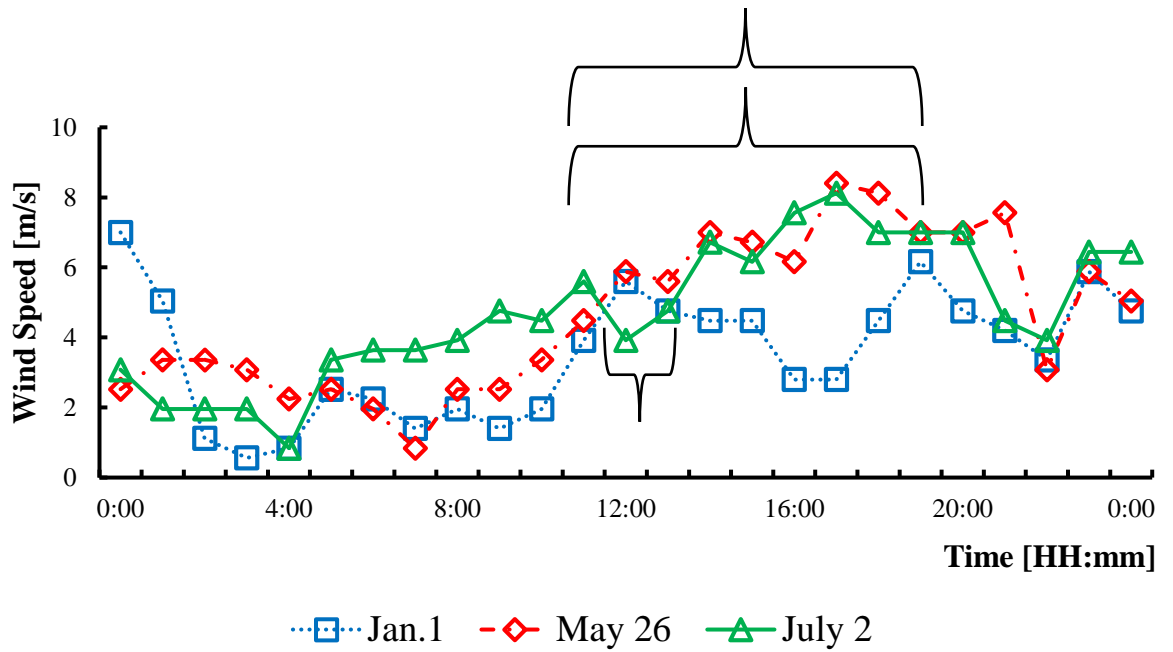


Figure 2. 2 Wind speed in Iqaluit for the day studied. The bracket shows the analysis period at QEC.

### 2.5.3 Estimation of PV Actual Output Efficiency

The PV array's output power data was obtained at 5-minute intervals whilst the ambient temperature and wind speed data were measured at 1-hour intervals. Hence, the ambient temperature and wind speed data were interpolated to estimate values at 5-minute intervals.

The PV arrays' estimated performance efficiencies and cell temperatures were calculated based upon the DC power and environmental weather using Equations 1, and 3-5. Initially, the solar irradiance on the tilted array was estimated by using the reference efficiency in Equation 1. Using the ambient temperature as the initial estimate of the PV cell temperature, the radiation heat loss from the array was estimated using Equation 7 and convection heat loss by the array was estimated using Equation 15. Then the cell temperature was estimated using Equation 4. In the next iteration, the electrical efficiency was immediately recalculated by Equation 3 using the new cell temperature. In subsequent iterations, the PV cell temperature was compared with the previous value and the iterations

stopped when it changed less than 0.1 K. Figure 3 shows the calculation sequence. In addition, the following were assumed in performing the calculations:

1. Convection and radiation heat losses are taking place from the top and bottom of the PV arrays. The convection heat loss coefficient is the same for the top and bottom.
2. Convection and radiation heat losses from the edges and sides of the array are negligible.
3.  $\tau\alpha = 0.9$  [34].
4. The glass temperature is equal to the PV cell temperature, and the ground and wall temperatures are equal to the ambient temperature [36].
5. Initially, the sky temperature was estimated using the Swinbank model (Equation 12), the view factors from Table 2.1 were used, and Equation 16 was used to calculate the heat transfer coefficient.

The overall heat loss coefficient  $U_{L,NOCT}$  under the NOCT situation was estimated using the same equations as used to estimate the overall heat loss coefficient,  $U_L$ . However, a wind speed of 1 m/s was used at NOCT conditions, but when estimating the overall heat loss coefficient under field conditions ( $U_L$ ) the measured wind speed was used. In order to separate the effect of the wind, another calculation was performed with a field wind speed of 1 m/s, effectively reducing the  $U_L/U_{L,NOCT}$  term in Equation 4 to unity and eliminating the wind effect.

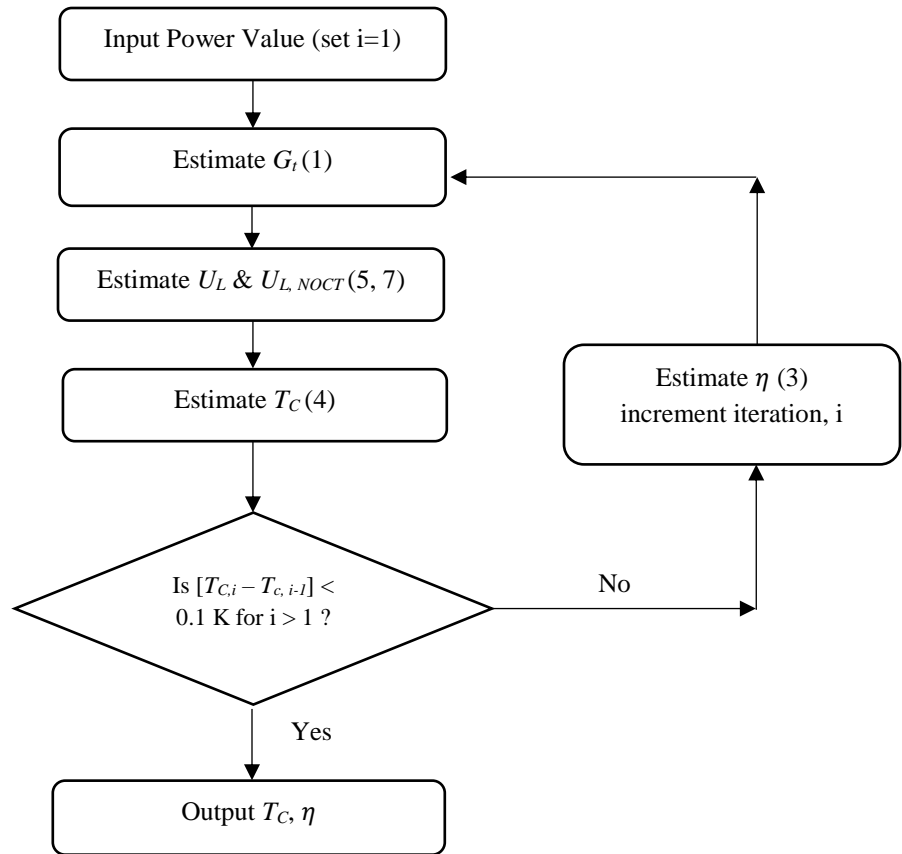


**Figure 2.3 Flow chart showing iterative calculation of  $T_c$  and  $\eta$ . Numbers in brackets are relevant equations.**

#### 2.5.4 Sensitivity Analysis

A sensitivity analysis was performed to test the impact on the arrays' energy balances of the following assumptions/equations:

1. The convective heat transfer coefficient equations of Charlesworth & Sharples (Equation 17) and Sturrock & Cole (Equation 18) using the Swinbank sky temperature model (Equation 12).
2. The three mentioned convective heat transfer coefficient equations (Equations 16, 17 and 18) with the Bliss sky temperature model (Equation 13).

3. The three mentioned convective heat transfer coefficient equations (Equations 16, 17 and 18), and two sky temperature models (Equations 12 and 13), with view factors  $F_1 = F_2 = 0.5$ .

## **2.6 Results and Discussion**

Figures 2.4 and 2.5 show a plot of the arrays' estimated efficiencies on January 1, 2017 when both radiation to the sky and wind-induced convection to the ambient air are considered versus the case with radiation to the sky and wind-induced convection to the ambient with a speed of 1 m/s. A detailed analysis is shown for January 1 because it was the coldest day of the study period. The estimated PV efficiency when both convection to the ambient air and radiation to the sky were considered together was within the range of 18.7% to 18.8% at QEC, whilst at AWGA it was 19.1%. This represents an 18% increase over that at the rated efficiency. However, when only radiation to the sky and convection at 1 m/s was considered, the estimated PV efficiencies dropped at both arrays by less than 0.5%, on average compared to the case with radiation and wind. Hence, the effect of convection to the ambient air was minimal on a winter day.

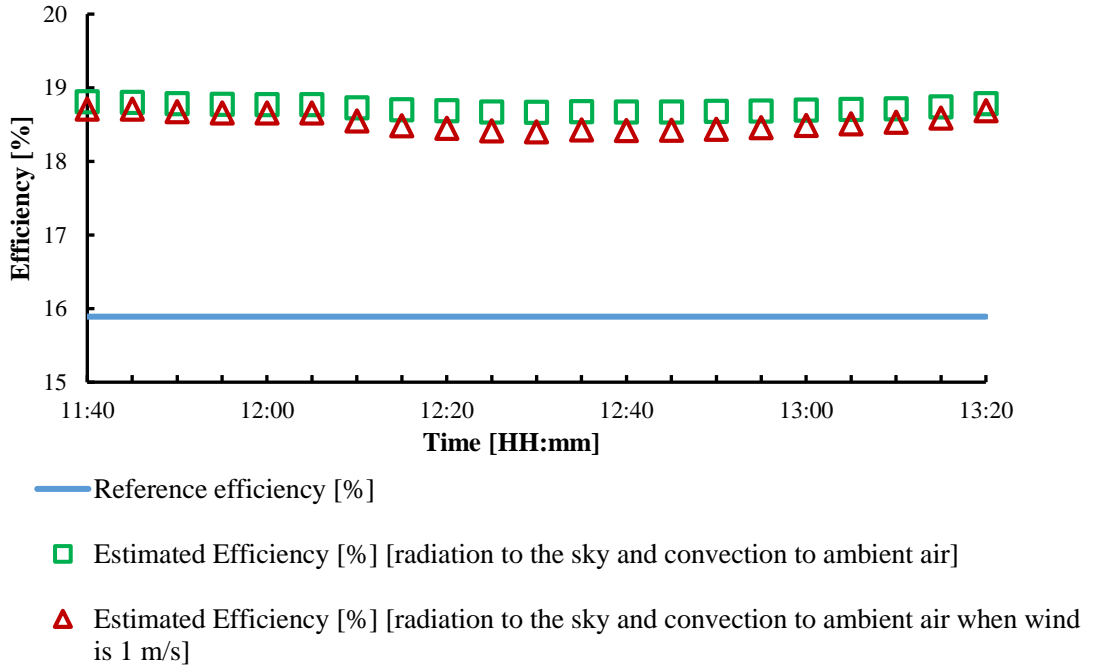


**Figure 2. 4 Reference and estimated PV efficiencies at QEC on January 1, 2017**

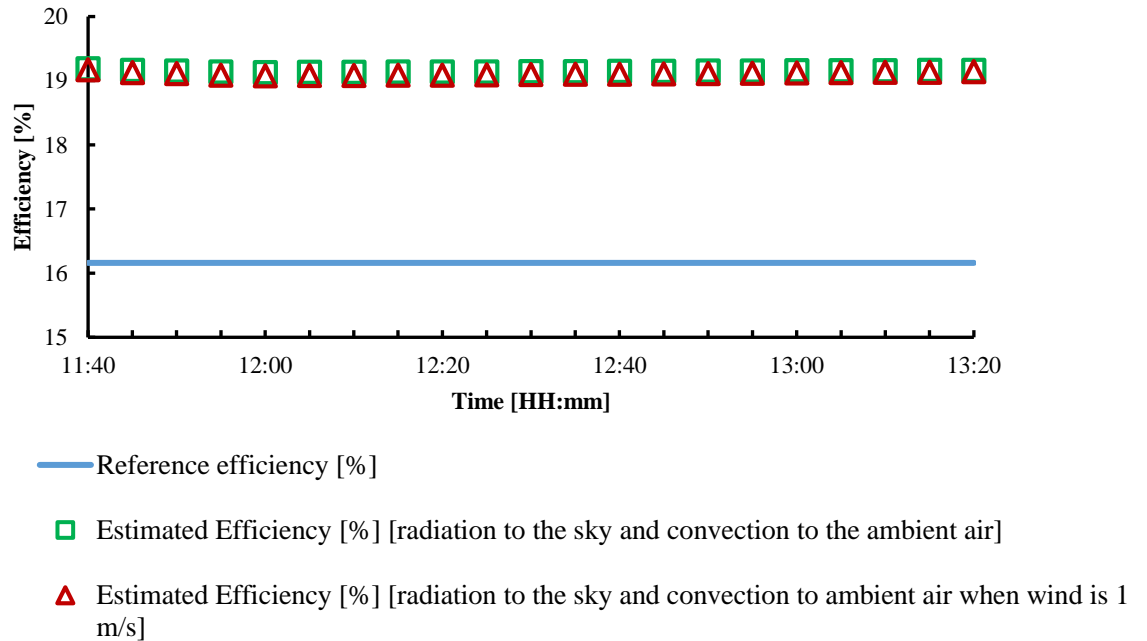


**Figure 2. 5 Reference and estimated PV efficiencies at AWGA on January 1, 2017**

Table 2.3 shows a summary of the estimated efficiencies and heat loss per area for the arrays at QEC and AWGA for the study period. On all three days under analysis,

when both convection to the ambient air and radiation to the sky were considered, both arrays were generating above their reference efficiencies. At QEC, the estimated efficiency averaged 18.8% on the clear and sunny winter day, whilst on the clear and sunny spring and summer days it was 16.9% and 16.1% respectively. At AWGA for the same days, the average efficiencies were 19.1%, 17.4% and 16.7%, respectively. When only radiation to sky and ambient air at 1 m/s was considered it was found that at QEC, the estimated efficiency on the clear and sunny winter day averaged at 18.7%, whilst on the clear and sunny spring and summer days the values were 16.0% and 15.2%, respectively. At AWGA for the same days the average estimated efficiencies were 19.1%, 17.0% and 16.4%, respectively. The effect of the convection to ambient air on the PV efficiencies was found by subtraction. At QEC, the convection to the ambient air ranged from 0.1% on the clear and sunny winter day to 0.9% on the clear and sunny spring and summer days whilst at AWGA there was no impact on the clear and sunny winter day and 0.4% and 0.3% on the clear and sunny spring and summer days of the study period. Hence, the estimated impact of convection to the ambient air on the estimated PV efficiencies was found to be below 1% in absolute terms on all three days for both arrays. Overall, the enhancement in efficiency at QEC resulted in an output that was 1.18 times the rated value on January 1. Similarly, AWGA experienced a 18% relative increase in output power for January 1.

**Table 2.3. Estimated performance summary for both arrays**

Description	QEC			AWGA		
	Jan. 1	May 26	July 2	Jan. 1	May 26	July 2
Mean Power [W]	584	1993	1851	758	3974	3384
Mean Temp. [°C]	-19.4	3.5	14.5	-19.4	3.5	14.5
Mean Wind speed [m/s]	4.9	6.3	6.3	4.9	6.3	6.3
PV rated $\eta$ [%]	15.89	15.89	15.89	16.16	16.16	16.16
Mean Estimated $\eta^*$ [%]	18.8	16.9	16.1	19.1	17.4	16.7
Mean Estimated $\eta^{**}$ [%]	18.7	16.0	15.2	19.1	17.0	16.4
Mean Estimated $\eta^{***}$ [%]	0.1	0.9	0.9	0	0.4	0.3
Mean $q_{rad}$ [W/m <sup>2</sup> ]	73.6	107.4	109.1	47.3	88.3	84.0
Mean $q_{conv.}$ [W/m <sup>2</sup> ]	59.1	380.4	380.4	0	190.5	165.4

\* mean estimated efficiency with both radiation to sky and convection to the ambient air  
 \*\* mean estimated efficiency with radiation to sky and convection to the ambient at 1 m/s  
 \*\*\* mean estimated efficiency difference between \* and \*\*  
 $q_{rad.}$  is mean estimated radiation heat flow  
 $q_{conv.}$  is mean estimated convection heat flow

## 2.6.1 Energy Balance

### 2.6.1.1 Base Case

Figures 2.6 and 2.7 show a plot of the mean estimated input and output energy flows for the arrays at QEC and AWGA, respectively, for the analysis period. On all three days, the mean estimated energy output was less than the mean estimated energy input at both arrays, thus resulting in a positive error in the estimated energy balance (Equation 19). At QEC, the error ranged from 8% to 9% whilst at AWGA it was from 3% to 6%. On the clear and sunny winter day, radiation to the sky was the more dominant heat loss mode, whilst on the clear and sunny spring and summer days it was convection to the ambient air. The reason for the sudden flip from radiation to convection was

primarily due to a significant rise in temperature difference between the PV cell and ambient air ( $\Delta T$ ) and a marginal increase of the convective heat transfer coefficient ( $h$ ) due to the increase in induced wind speed from a mean of 4.9 m/s on the winter day to 6.3 m/s on the spring and summer days. Figure 2.8 shows graphically how the heat loss elements from QEC array changed during the seasons. The radiation temperature difference ( $RTD = T_C^4 - T_S^4$ ) increased by less than twice from winter to spring and summer, however, the change in  $\Delta T = T_C - T_a$  was greater than seven times. At AWGA the situation is similar to QEC. Some heat flows that were neglected in this analysis that may have caused the mean estimated input energy flow to be greater than the output are: conduction heat loss from the PV panels to the mounting brackets, and radiation and convection from the sides (edges) of the PV panels.

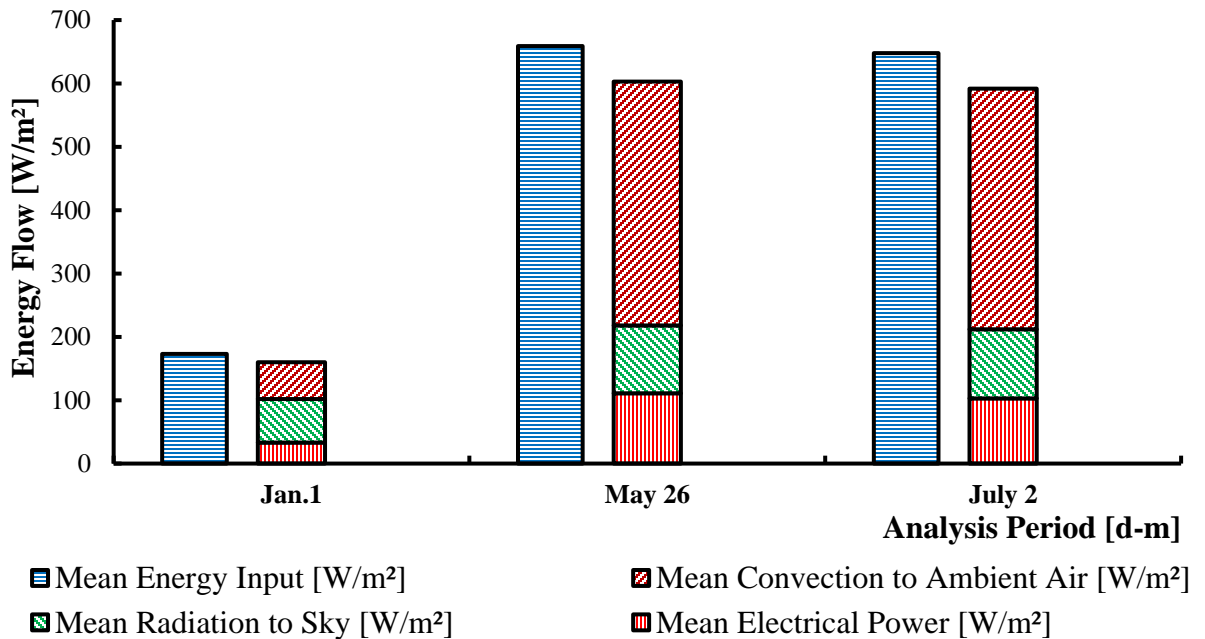


Figure 2. 6 Energy balance at QEC during the analysis period

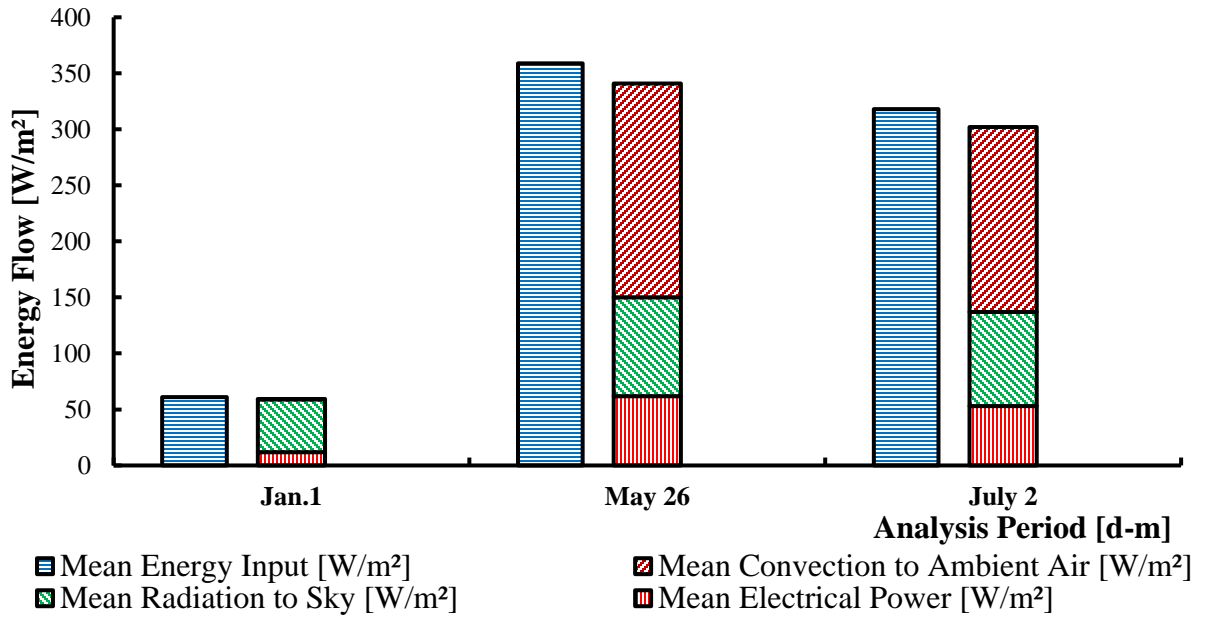


Figure 2. 7 Energy balance at AWGA during the analysis period

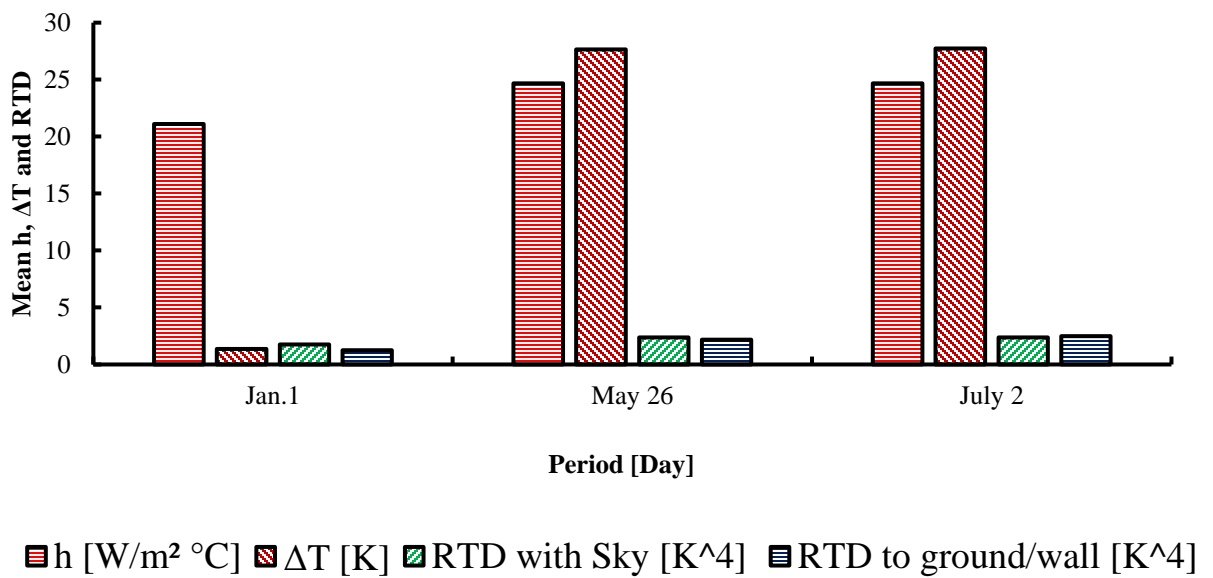


Figure 2. 8 Mean change in h, ΔT and RDT at QEC for analysis period. RTD value has been multiplied by 10<sup>9</sup>.

### 2.6.1.2 Sensitivity

Figures 2.9, 2.10, 2.11 and 2.12 show plots of the estimated mean energy balance error (Equation 19) for both QEC and AWGA arrays for the analysis period for the

conditions outlined earlier under Section 2.5.4 (Sensitivity Analysis). In Figure 2.9, Charlesworth & Sharples (Equation 17) and Sturrock & Cole (Equation 18) convective heat transfer coefficient models were tested against the base case convective heat transfer coefficient formula (Test *et al.*), using the Swinbank sky temperature model (Equation 12). At QEC, Charlesworth & Sharples gives an estimated error ranging from 14% to 16%, while for Sturrock & Cole the error ranges from 32% to 36%. These are both more than the base case (Test *et al.*) which has an error of 8% to 9%. At AWGA the estimated error ranges from 3% to 12% and 3% to 32% for Charlesworth & Sharples and Sturrock & Cole, respectively and again, the Test *et al.* model had the lowest error. The lower error indicates a more accurate convection heat transfer model, which implies a more accurate estimate of PV cell temperature and efficiency.

In Figure 2.10, the estimated energy balance error for all three convective heat transfer coefficient models (Equations 16, 17 and 18) were calculated using the Bliss model (Equation 13) to estimate sky temperature. At QEC, the estimated error was 9% when using the Test *et al.* model which is similar to the result using the Swinbank sky model. At AWGA for the same period and sequence, the estimated error ranged from -23% to 6% when using the Test *et al.* model. Negative errors indicate that the mean estimated energy input is less than the mean estimated energy output, which would not result from neglecting selected heat transfer losses.

In Figure 2.11, the estimated energy balance errors for all three convective heat transfer coefficient models (Equations 16, 17 and 18) were calculated using the Swinbank sky model (Equation 12) and array view factors ( $F_1$  and  $F_2$ ) of 0.5. At QEC, using the Test *et al.* model, the estimated error was 8% to 9%. Whilst at AWGA for the same

period and sequence, the estimated errors ranged from 7% to 28%. Hence, when compared to the base case models there was no reduction in the estimated error with the new view factors, and for AWGA the error was considerably higher.

In Figure 2.12, the estimated energy balance error for all three convective heat transfer coefficient models (Equations 16, 17 and 18) were calculated using the Bliss sky model (Equation 12) and array view factors of 0.5. At QEC, using the Test *et al.* model, the estimated error was 9%, which is similar to the base case. While at AWGA, the estimated errors ranged from 7% to 28%. Hence, when compared to the base case models it was found that the base case models had the least estimated error.

Therefore, the base case models (Test *et al.* convective heat transfer coefficient, Swinbank sky temperature and Armstrong and Hurley view factors) yield the least estimated energy balance error, thus are considered the most accurate in terms of estimating the energy balance for an array located in cold climate.

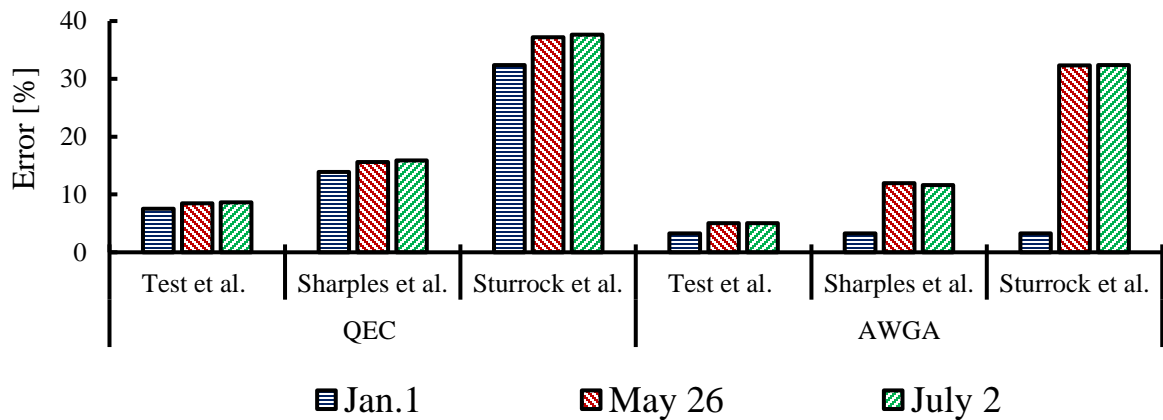


**Figure 2.9 Energy balance error at QEC and AWGA for the analysis period. (Swinbank sky temperature model and three convective heat transfer models)**

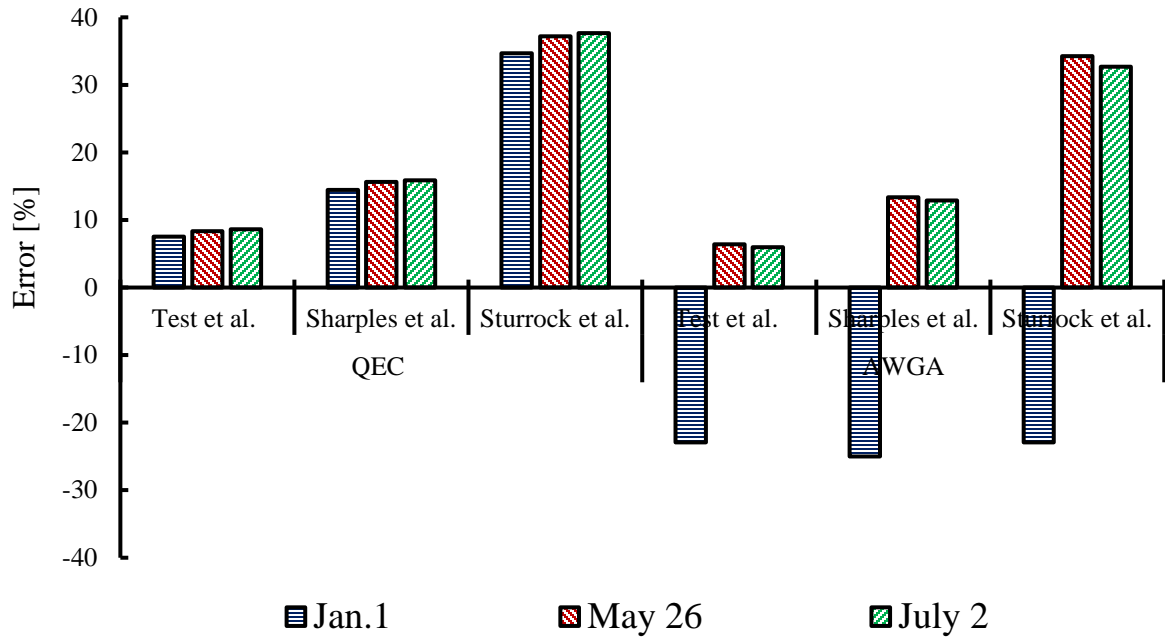


Figure 2.10 Energy balance error at QEC and AWGA for the analysis period. (Bliss sky temperature model and three convective heat transfer models)

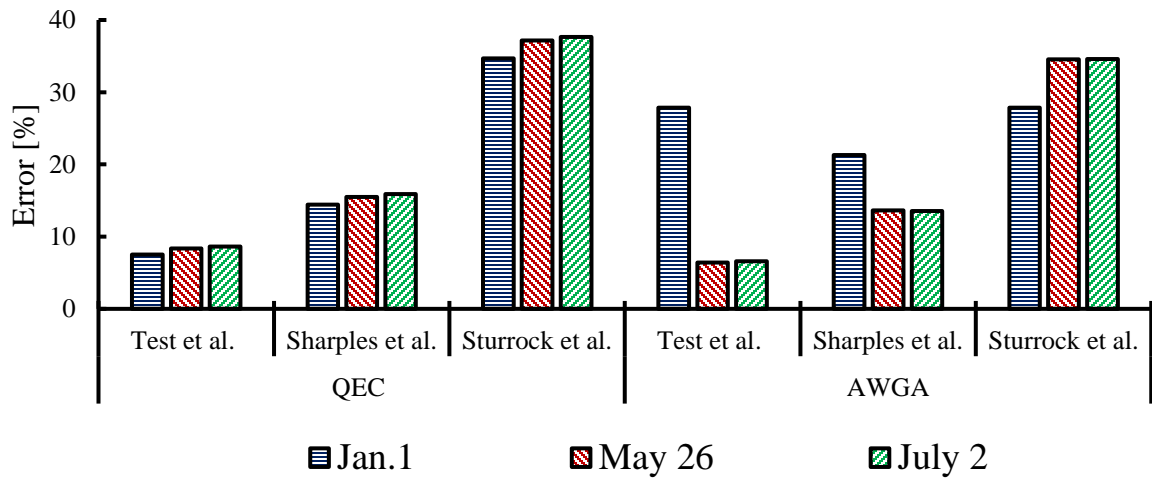


Figure 2.11 Energy balance error at QEC and AWGA for the analysis period. ( $F_{top-sky}=0.5$ , Swinbank sky temperature model and three convective heat transfer models)

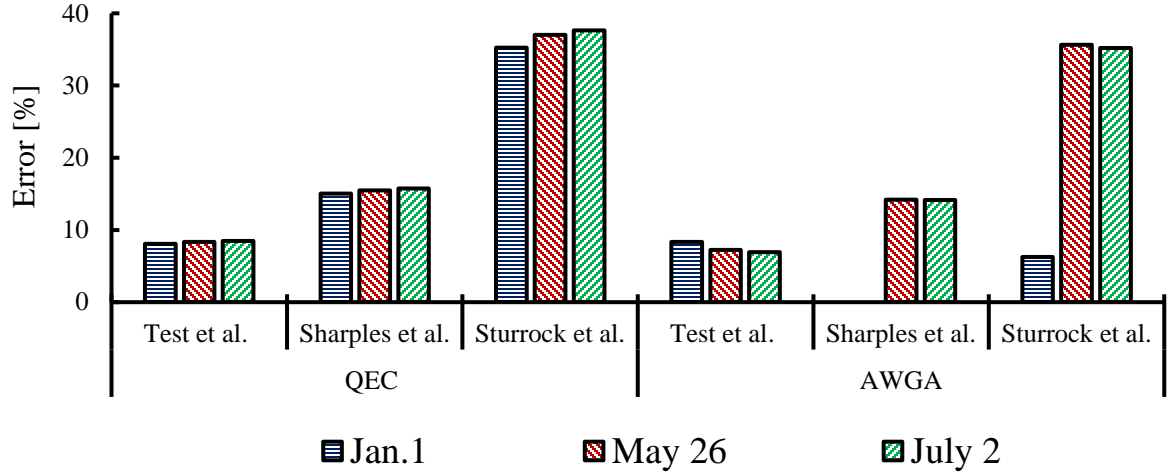


Figure 2.12 Energy balance error at QEC and AWGA for the analysis period. ( $F_{top-sky}=0.5$ , Bliss sky temperature model and three convective heat transfer models)

## 2.6.2 Mean Annual Average

Tables 2.4 and 2.5 show a summary of the estimated performance and energy-weighted efficiency enhancements for both arrays for a clear and sunny day in each month of 2017. The results indicate that both arrays are over performing above their rated efficiencies in this climate. The relative efficiency enhancement (REE) was calculated using Equation 20.

$$REE = \left( \frac{\eta_{daily\ mean\ est.} - \eta_{rated}}{\eta_{rated}} \right) \times 100\% \quad (20)$$

Arithmetically averaging the twelve values of  $REE$ , it was found that at QEC, the annual mean relative enhancement efficiency was 10% while for the same period at AWGA it was 11%. However, a more meaningful *energy-weighted average* ( $REE_{ewa}$ ) would take into account the energy produced in each month. Thus, was calculated using Equation 21.

$$REE_{ewa} = \left( \frac{\sum_{i=1}^{12} E_i \times REE_i}{\sum_{i=1}^{12} E_i} \right) \times 100\% \quad (21)$$

where  $E_i$  is the mean energy (Wh) and REE (%) is the relative efficiency enhancement for the clear and sunny day in each month of 2017.

The mean annual energy-weighted efficiencies were 4% at QEC and 7% at AWGA.

**Table 2.4 1. Calculation of monthly energy-weighted relative efficiency enhancement at QEC (reference  $\eta = 15.89\%$ )**

Description	Months											
	Jan. 1	Feb. 2	Mar. 6	Apr. 4	May 26	June 1	July 2	Aug. 15	Sept. 18	Oct. 1	Nov. 3	Dec. 5
$\eta$ daily mean est. [%]	18.8	19.6	18.8	17.6	16.9	17.0	16.1	15.9	16.5	17.1	17.7	17.9
REE [%]	18.3	23.3	18.3	10.8	6.4	7.0	1.3	0.0	3.8	7.6	11.4	12.6
REE <sub>ewa</sub> [%]	1.0	1.0	9.0	13.0	8.0	8.0	1.0	0.0	3.0	6.0	3.0	0.0

**Table 2.5. Calculation of monthly energy-weighted relative efficiency enhancement at AWGA (reference  $\eta = 16.16\%$ )**

Description	Months											
	Jan. 1	Feb. 2	Mar. 6	Apr. 4	May 26	June 1	July 2	Aug. 15	Sept. 18	Oct. 1	Nov. 3	Dec. 5
$\eta$ daily mean est. [%]	19.1	19.8	19.3	18.3	17.4	17.6	16.7	16.5	17.1	17.4	18.2	18.1
REE [%]	18.2	22.5	19.4	13.2	7.7	8.9	3.3	2.1	5.8	7.7	12.6	12.0
REE <sub>ewa</sub> [%]	1.0	0.0	1.0	20.0	13.0	16.0	5.0	3.0	8.0	11.0	6.0	2.0

Figure 2.13 shows a plot of the estimated efficiencies for both arrays (QEC and AWGA) for a clear and sunny day in each month of the year (January to December, 2017) versus literature efficiencies outlined in Section 2.2. As the ambient temperature becomes colder the estimated efficiency for both arrays increased compared to their reference efficiencies. However, the slope of the literature results is greater which reflects

the fact that monocrystalline PV modules have a greater temperature co-efficient than polycrystalline modules, as exist at QEC and AWGA.

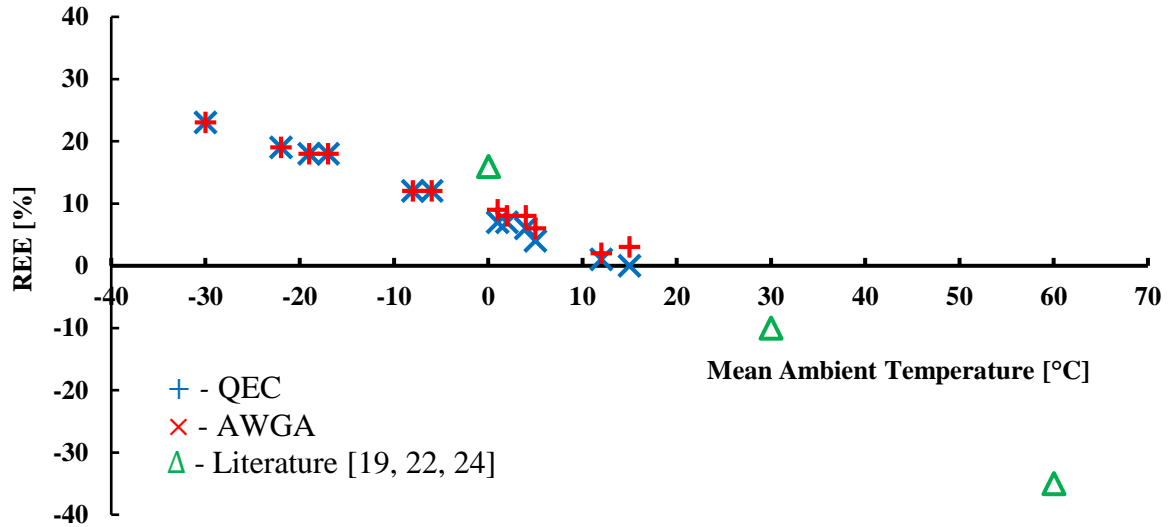


Figure 2.13 Mean monthly relative efficiency enhancements for both arrays compared to literature projects

## 2.7 Conclusion and Future Plans

These analyses estimated the output performance of the two PV arrays in Arctic conditions on sunny days in 2017. Based on the estimated results it can be concluded that both arrays are performing above their rated capacity by 4% to 7% on a mean annual energy-weighted basis. An energy balance was performed, considering radiation to the sky and convection to ambient air. During the winter days radiation to the sky was the dominant heat loss mode in cooling of the PV cells while during the other seasons, convection to the ambient air was the dominant heat loss mode.

In calculating the heat loss from the PV array, it was found that the Test *et al.* convection heat transfer coefficient model, the Swinbank sky temperature model, and the Armstrong and Hurley view factors provided the least error in the energy balance. The

lower error gives more confidence that all significant heat losses were considered. Future work will attempt to estimate the horizontal solar irradiance (G) at a location based on measured power output from multiple PV arrays with different orientations

## REFERENCES

- [1] S. Kalogirou, Solar Energy Engineering, in: Processes and Systems, Elsevier Inc., Burlington, MA, 2009
- [2] L. Yang, X. Gao, F. Lv, X. Hui, L. Ma, X. Hou, Study on the local climatic effects of large photovoltaic solar farms in desert areas, *Solar Energy* 144 (2017) 244–253.
- [3] M. Bayrakci, Y. Choi, J.R.S Brownson, Temperature dependent power modeling of photovoltaics, *Energy Procedia* 57 (2014) 745–754.
- [4] M. Habibollahi, M. Ameri, S.H. Mansouri, Efficiency improvement of photovoltaic water pumping systems by means of water flow beneath photovoltaic cells surface, *Journal of Solar Energy Engineering* 137-4 (2015) 044501.
- [5] T. Ma, W. Gu, L. Shen, L. M. Li, An improved and comprehensive mathematical model for solar photovoltaic modules under real operating conditions, *Solar Energy* 184 (2019) 292–304.
- [6] K. Earley, Why renewables are winning the ‘carbon war’, *Renewable Energy Focus* 19-20 (2017) 117-120.
- [7] B. Bora, R. Kumar, O.S. Sastry, B. Prasad, S. Mondal, A.K. Tripathi, Energy rating estimation of PV module technologies for different climatic conditions, *Solar Energy* 174 (2018) 901–911.
- [8] S. Ghosh, V.K. Yadav, V. Mukherjee, Impact of environmental factors on photovoltaic performance and their mitigation strategies—A holistic review, *Renewable Energy Focus* 28 (2019) 153-172.

- [9] J. M. Pearce, S.V. Obydenkova, Technical viability of mobile solar photovoltaic systems for indigenous nomadic communities in northern latitudes, *Renewable Energy* 89 (2016) 253–267.
- [10] L. Dignard-Bailey, S. Martel, M.M.D. Ross, Photovoltaics for the North: A Canadian Program, 2nd World Conference and Exhibition on Photovoltaic Solar Energy Conversion Vienna, Austria (1998).
- [11] M. Ross, Photovoltaics in cold climates, in: James & James, Science Publishers Ltd, 1999, pp. 16–20.
- [12] W.Tian, Y. Wang, J. Ren, L. Zhu, Effect of urban climate on building integrated photovoltaics performance, *Energy Conversion and Management* 48 (2007) 1–7.
- [13] N. Bowman, S. Shaari, Photovoltaics in buildings: A case study for rural England and Malaysia, *Renewable Energy* 15 (2002) 558–561.
- [14] E. Skoplaki, A.G. Boudouvis, J.A. Palyvos, A simple correlation for the operating temperature of photovoltaic modules of arbitrary mounting, *Solar Energy Materials and Solar Cells* 92 (2008) 1393–1402.
- [15] P. Trinuruk, C. Sorapipatana, D. Chenvidhya, Estimating operating cell temperature of BIPV modules in Thailand, *Renewable Energy* 34 (2009) 2515–2523.
- [16] J.L. Balenzategui, M.C. Alonso García, Estimation of photovoltaic module yearly temperature and performance based on nominal operation cell temperature calculations, *Renewable Energy* 29 (2004) 1997–2010.

- [17] E. Skoplaki, J. A. Palyvos, On the temperature dependence of photovoltaic module electrical performance: A review of efficiency/power correlations, *Solar Energy* 83 (2009) 614–624.
- [18] E. Skoplaki, J. A. Palyvos, Operating temperature of photovoltaic modules: A survey of pertinent correlations, *Renewable Energy* 34 (2009) 23–29.
- [19] Latitude, Iqaluit Nunavut Canada Latitude. <http://latitude.to/articles-by-country/ca/canada/1534/iqaluit>, (accessed 7 May, 2018).
- [20] M. Mussard, Solar energy under cold climatic conditions: A review, *Renewable and Sustainable Energy Reviews* 74 (2017) 733–745.
- [21] L.S. Pantic, T.M. Pavlović, D.D. Milosavljević, I.S. Radonjic, M.K. Radovic, G. Sazhko, The assessment of different models to predict solar module temperature, output power and efficiency for Nis, Serbia, *Energy* (2016) 38–48.
- [22] A. Kasaeian, Y. Khanjari, S. Golzari, O. Mahian, S. Wongwises, Effects of forced convection on the performance of a photovoltaic thermal system: An experimental study, *Experimental Thermal and Fluid Science* 85 (2017) 3–21.
- [23] Z. Peng, M.R. Herfatmanesh, Y. Liu, Cooled solar PV panels for output energy efficiency optimisation, *Energy Conversion and Management* 150 (2017) 949–955.
- [24] J.D. Mondol, Y. Yohanis, M. Smyth, B. Norton, Long term performance analysis of a grid connected photovoltaic system in Northern Ireland, *Energy Conversion and Management*, 47-18 (2006) 2925–2947.

- [25] A. Vassel & F. Iakovidis, The effect of wind direction on the performance of solar PV plants, *Energy Conversion and Management* 153 (2017) 455–461.
- [26] I. El-Amin, S. Rehman, Performance evaluation of an off-grid photovoltaic system in Saudi Arabia, *Energy* 46-1 (2012) 451–458.
- [27] F. Fouladi, P. Henshaw, P. D.S-K. Ting, Enhancing smart grid realisation with accurate prediction of photovoltaic performance based on weather forecast, *International Journal of Environmental Studies* 70-5 (2013) 754–764.
- [28] Spectrolab Inc. Sylmar C.A, Photovoltaic Systems Concept Study: Final Report (ALO-2748-12), Springfield, VA: US Department of Energy, Division of Solar Energy (1977).
- [29] D.L. Evans, Simplified method for predicting photovoltaic array output, *Solar Energy* 27-6 (1981) 555–560.
- [30] H. Sainthiya, N.S. Beniwal, N. Garg, Efficiency improvement of a photovoltaic module using front surface cooling method in summer and winter conditions, *Journal of Solar Energy Engineering*, 140-6 (2018) 061009.
- [31] International Electrotechnical Commission, Crystalline silicon terrestrial photovoltaic (PV) modules – Design qualification and type approval, second ed, Geneva: IEC, International Standard EN-61215, 1993-04 (1993).

- [32] B. Hüttl, L. Gottschalk, S. Schneider, D. Pflaum, A. Schulze, Accurate performance rating of photovoltaic modules under outdoor test conditions, *Solar Energy* 177 (2019) 737–745.
- [33] E. Rossi, H. Ossenbrink, European solar test installation: Qualification test procedures for crystalline silicon photovoltaic modules (ISSN 1018-5593), Commission of the European Communities (1992).
- [34] N. Aste, G. Chiesa, F. Verri, Design, development and performance monitoring of a photovoltaic-thermal (PVT) air collector, *Renewable Energy* 33-5 (2008) 915–927.
- [35] J.A. Duffie, W. A. Beckman, W. A., *Solar Engineering of Thermal Processes*, second ed., John Wiley and Sons, New York, 1980.
- [36] S. Armstrong, W.G. Hurley, A thermal model for photovoltaic panels under varying atmospheric conditions, *Applied Thermal Engineering* 30 11-12 (2010) 1488–1495.
- [37] G. Notton, C. Cristofari, M. Mattei, P. Poggi, Modelling of a double-glass photovoltaic module using finite differences, *Applied Thermal Engineering* 25 (2005) 2854–2877.
- [38] W.C. Swinbank., Long-wave radiation from clear skies, *Quarterly Journal of the Royal Meteorological Society* 89 (1963).
- [39] R.W. Bliss, Atmospheric radiation near the surface of the ground: A summary for engineers, *Solar Energy* 5-3 (1961) 103–120.

[40] F.L. Test, R.C. Lessmann, A. Johary, Heat transfer during wind flow over rectangular bodies in the natural environment, *Journal of Heat Transfer* 262-103 (2009) 262–267.

[41] P.S. Charlesworth, S. Sharples, Full-scale measurements of wind-induced: Convective heat transfer from a roof mounted flat plate solar collector, *Solar Energy* 62-2 (1998) 69–77.

[42] N. S. Sturrock, R. J. Cole, The convective heat exchange at the external surface of buildings, *Building and Environment* 12 (1977) 207–214.

[43] M.K. Fuentes, A simplified thermal model for flat-plate photovoltaic arrays, Sandia Report (SAND85-0330) UC-63 (1987).

[44] Environment and Natural Resources, Gov't of Canada, Hourly data report for Iqaluit Climate, 2017.

[http://climate.weather.gc.ca/climate\\_data/hourly\\_data\\_e.html?hlyRange=2004-12-16%7C2018-06-11&dlyRange=2004-05-25%7C2018-06-10&mlyRange=2005-03-01%7C2007-11-01&StationID=42503&Prov=NU&urlExtension=e.html&searchType=stnName&optLimit=yearRange&StartYear=1840&EndYear=2013&selRowPerPage=25&Line=2&searchMethod=contains&Month=1&Day=31&txtStationName=iqaluit&timeframe=1&Year=2017](http://climate.weather.gc.ca/climate_data/hourly_data_e.html?hlyRange=2004-12-16%7C2018-06-11&dlyRange=2004-05-25%7C2018-06-10&mlyRange=2005-03-01%7C2007-11-01&StationID=42503&Prov=NU&urlExtension=e.html&searchType=stnName&optLimit=yearRange&StartYear=1840&EndYear=2013&selRowPerPage=25&Line=2&searchMethod=contains&Month=1&Day=31&txtStationName=iqaluit&timeframe=1&Year=2017) (accessed 4 June, 2018).

[45] Google Maps, Map of Iqaluit, Nunavut, Canada showing direction.

<https://www.google.com/maps/dir///@42.2926058,-83.0770962,15z> (accessed 18 July, 2018)

[46] J.-P. Pinard, Potential for Wind Energy in Nunavut Communities.

[https://www.qec.nu.ca/sites/default/files/potential\\_for\\_wind\\_energy\\_in\\_nunavut\\_communities\\_2016\\_report\\_0.pdf](https://www.qec.nu.ca/sites/default/files/potential_for_wind_energy_in_nunavut_communities_2016_report_0.pdf) , 2016 (accessed 8 July, 2018)

[47] Jinko Solar, JKM260PP-60 Poly crystalline module 240-260 Watts.

[https://www.jinkosolar.com/ftp/EN-Eagles-260PP\\_v1.0\\_rev2013.pdf](https://www.jinkosolar.com/ftp/EN-Eagles-260PP_v1.0_rev2013.pdf) , 2013 (accessed 7 May, 2018).

[48] C.S.I. , ClearPower CS6P-260/265P-SD.

[https://www.canadiansolar.com/downloads/datasheets/v5.4/Canadian\\_Solar-Datasheet-CS6PPSD\\_SmartDC-v5.4en.pdf](https://www.canadiansolar.com/downloads/datasheets/v5.4/Canadian_Solar-Datasheet-CS6PPSD_SmartDC-v5.4en.pdf) , 2016 (accessed 7 May, 2018).

## CHAPTER 3

### PREDICTING THE HORIZONTAL SOLAR IRRADIANCE (G) FROM MEASURED PV OUTPUT POWER IN SUB-ARCTIC CLIMATE

#### **3.1 Introduction**

Renewable energy is available in numerous forms such as solar, wind, hydropower, geothermal and biomass [1-2]. The last decade saw a rapid incline of solar photovoltaic (PV) technology used in the generation of electricity globally [3-4]. Solar PV cells are semi-conductor devices which convert the energy from the sunlight directly into electricity [5]. The driving factors for the rapid incline of solar PV are zero emission of greenhouse gases, policies and strategies from governments in countries around the world, desire for energy independence, and reduced per unit cost for solar panels [6-11]. For any country to have growth and sustainability, it is important that reliable energy is always available [12]. At the same time, forecasted energy demand figures show that the world electricity peak demand by the year 2035 will increase to almost twice what it was in 2008, to approximately 32.9 TW. Thus, renewable energy resources can play a great role in meeting the future world energy demand. One forecast sees solar PV technologies as meeting greater than 93% of that energy demand [13-14].

Further, solar PV arrays are considered to be an economical way to offset fuel costs for communities where the cost of fossil fuels is very expensive due to limited transportation options [15]. Many of the northern communities in Canada fit directly into this category, since these communities are not connected to the national grid and receive almost all of their electrical energy from diesel generators. This dependency on fossil fuels results in electrical utilities with high operational and environmental costs.

Increasing the use of renewable energy, such as solar PV technologies will support energy sustainability and future development of these northern communities [16].

When designing and developing solar PV projects, it is very critical to know the solar energy available at the site. A commonly tabulated parameter is the horizontal solar irradiance ( $G$ ) [17]. By knowing the value of  $G$  for the site, the designer is better equipped to estimate the solar PV array output and at the same time able to accurately size the system to harness the available energy from the sun. The horizontal solar irradiance includes both diffuse and direct (beam) components [17-18]. In addition, as to exploit the maximum energy from the sun, the solar PV arrays are installed or arranged with a tilt toward the equator [19]. The tilt from the horizontal decreases the incidence angle and increases the intensity of solar irradiance on the array. The sun incident angle is the angle between the normal to the surface and the sunlight ray. The tilt angle for fixed arrays is set to maximize either the annual output, seasonal output, or hourly output of the array. During the winter season the sun is at a lower solar altitude while in the summer it is at a higher solar altitude [19].

The pyranometer is an instrument used to measure solar irradiance at a location and is used to collect irradiation data for predicting the output of solar arrays. A full solar measurement station includes pyranometers for measuring total and diffuse radiation, as well as a pyrheliometer for measuring direct beam radiation. They are not commonly deployed due to their very high procurement cost, so the solar irradiation in most locations is determined by interpolation between stations, or using satellite data of cloud cover and theoretical calculations. Solar data north of  $58^\circ$  in Canada are sparse [20].

In this paper, analysis is done using the measured solar PV power output data from two separate solar PV arrays with different azimuths located in Iqaluit, Nunavut, Canada. Iqaluit is located close to the Arctic Circle, at a latitude of 63.75 degrees north, and is the capital of the territory of Nunavut [21]. In predicting the horizontal solar irradiance ( $G$ ) at the two locations for clear and sunny days in winter, spring and summer of 2017, the horizontal solar irradiance ( $G$ ) values were back-calculated from the solar irradiance on the tilted arrays ( $G_t$ ), sky clearness index ( $k_T$ ), and beam radiation tilt factor ( $R_b$ ). Another method, combining the equations for converting to  $G$  from  $G_t$  for the two arrays, was attempted, but gave poor results (Appendix C).

### 3.2 Basic Solar Components

When estimating the solar irradiance on the plane of an array ( $G_t$ ) for a location, it is necessary to determine the following basic solar components:

#### 3.2.1 Terrestrial Horizontal Solar Irradiance ( $G$ )

The terrestrial horizontal solar irradiance is defined as the entire shortwave radiation (W) received from the sun by a surface per unit area ( $m^2$ ) parallel to the ground. The terrestrial horizontal solar irradiance is the sum of beam and diffuse solar irradiances [22-23]:

$$G = G_b + G_d \tag{1}$$

##### A. Beam Irradiance on a Horizontal Surface ( $G_b$ )

The beam irradiance on a horizontal surface ( $G_b$ ) is the amount of radiation (in W) coming directly from the sun and received by a unit area of surface (in  $m^2$ ) that is parallel to the earth's surface [22-23]. The beam irradiance on a horizontal surface for a clear-sky can be estimated using the following equation [22-23]:

$$G_b = G_{on} \times \tau_b \times \cos\theta_Z \quad (2)$$

where  $G_{on}$  is defined as the extraterrestrial radiation reaching the earth's outer atmosphere, measured on a plane perpendicular to the sun's radiation on a particular day in the year and  $\tau_b$  is the atmospheric transmittance coefficient for the sun beam radiation and is estimated from the following equation [23-24]:

$$\tau_b = a_0 + a_1 e^{-k/\cos\theta_Z} \quad (3)$$

where  $\theta_Z$  is the zenith angle, and  $a_0$ ,  $a_1$  and  $k$  are constants for an atmosphere with a visibility of greater than 23 km and an altitude no more than 2.5 km and can be estimated from the following equations [23-24]:

$$\theta_Z = \sin(L)\sin(\delta) + \cos(L)\cos(\delta)\cos(\omega) \quad (4)$$

$$a_0 = 0.4237 - 0.00821(6 - A)^2 \quad (5)$$

$$a_1 = 0.5055 + 0.00595(6.5 - A)^2 \quad (6)$$

$$k = 0.2711 + 0.01858(2.5 - A)^2 \quad (7)$$

where  $L$ ,  $\delta$ ,  $\omega$  and  $A$  are the latitude, declination angle, hour angle and altitude (elevation) of the site in km, respectively.

#### B. Diffuse Horizontal Irradiance ( $G_d$ )

The diffuse horizontal irradiance ( $G_d$ ) is the irradiance (in W) received by a surface per unit area (in m<sup>2</sup>) that does not come directly from the sun, but has been dispersed by particles and gases present in the atmosphere. Thus the diffuse light is the illumination coming from the clouds and the clear sky [22-23]. The diffuse horizontal irradiance can be estimated using the following equation [22, 25-26]:

$$G_d = G_{On} \times \tau_d \times \cos\theta_z \quad (8)$$

where  $\tau_d$  is the atmospheric transmittance coefficient of the sun diffuse radiation and is estimated from the following Equation [22, 25-26]:

$$\tau_d = 0.2710 - 0.2939\tau_B \quad (9)$$

### 3.2 Hourly Sky Clearness Index ( $k_T$ )

The hourly sky clearness index is the ratio of the hourly terrestrial horizontal solar irradiation to the extraterrestrial horizontal solar irradiation for that same hour. Hence, it is dimensionless and ranges from 0 to 1 and is defined by the following equation [22-23]:

$$k_T = \frac{I}{I_o} \quad (10)$$

where  $I_o$  is the extraterrestrial horizontal irradiation (in kJ) and is defined as the solar irradiation falling on a horizontal (parallel to the ground) surface outside of the earth's atmosphere per hour per area ( $m^2$ ). Often irradiance ( $G$ ) values for the middle of the hour are multiplied by 3600s and used as hourly irradiation values ( $I$ ), or the hourly values are divided by 3600s to give an irradiance value which is assumed constant over the hour. In this paper, the ratio of hourly irradiation values ( $I/I_o$ ) is assumed equal to the ratio of irradiance values ( $G/G_o$ ) such that  $k_T \approx G/G_o$ .

Knowing that:

$$G_o = G_{on} \cos\theta_z \quad (11)$$

and substituting Equation 11 into Equations 2 and 8 and substituting the resulting equation into Equation 1 gives:

$$G = G_o(\tau_b + \tau_d) \quad (12)$$

Substituting Equation 12 into Equation 10 results in:

$$k_T \simeq \frac{G}{G_o} = \frac{G_o(\tau_b + \tau_d)}{G_o} = \tau_b + \tau_d \quad (13)$$

### 3.3 Methodology

#### 3.3.1 PV Output Power Data

The power output data were taken from two arrays installed in Iqaluit: Qulliq Energy Corporation (QEC) with an array size of 2.86 kW and Arctic Winter Games Arena (AWGA) with an array size of 10.4 kW. The data was collected for clear and sunny winter, spring and summer days for 2017. The data was retrieved from Fronius IG plus 10 kW Inverters (Wels, Austria) which are remotely monitored by Green Sun Rising Incorporated (solar designers and contractors in Windsor, Ontario, Canada). However, for the analysis period a threshold of 300 W was implemented, such that the time when the output was greater than and equal to 300 W was considered for the analysis. The reason for the threshold of 300 W was due to significant power fluctuation under low solar altitude conditions, thus making it difficult to analyze. For comparison, during the winter solstice, the average day in Iqaluit lasts approximately 4 ½ hours while at the summer solstice it is approximately 20 hours.

#### 3.3.2 Estimation of Hourly Horizontal Solar Irradiance ( $G$ )

The PV array's DC output power data was obtained at 5-minute intervals while the ambient temperature and wind speed data were measured at 1-hour intervals. The solar

irradiance on the horizontal surface ( $G$ ) for both arrays at QEC and AWGA were calculated based upon a 5-minute interval using the following Equation [1]:

$$G = \frac{G_t}{\left\{R_b \left[1 - \frac{G_D}{G}\right] + \frac{G_D}{G} \left[\frac{1 + \cos\beta}{2}\right] + \rho_G \left[\frac{1 - \cos\beta}{2}\right]\right\}} \quad (14)$$

And [1, 23]:

$$R_b = \frac{\cos\theta}{\cos\theta_z} \quad (15)$$

$R_b$  and  $\theta$  are the beam radiation tilt factor and sun incident angle, respectively. The sun incident angle is estimated from the following Equation [22-23]:

$$\begin{aligned} \cos(\theta) = & \sin(L)\sin(\delta)\cos(\beta) - \cos(L)\sin(\delta)\sin(\beta)\cos(\theta_\gamma) + \\ & \cos(L)\cos(\delta)\cos(\omega)\cos(\beta) + \sin(L)\cos(\delta)\cos(\omega)\cos(\beta) + \\ & \sin(L)\cos(\delta)\cos(\omega)\sin(\beta)\cos(\theta_z) + \cos(\delta)\sin(\omega)\sin(\beta)\sin(\theta_\gamma) \end{aligned} \quad (16)$$

Where  $\beta$  and  $\theta_\gamma$  are PV tilt and azimuth angle, respectively. The tilt angle for both arrays are  $60^\circ$  while the azimuth angle is  $11.3^\circ$  at AWGA and  $45^\circ$  at QEC (Appendix A).

In estimating the horizontal solar irradiance ( $G$ ), it is necessary to estimate the ratio of the diffuse irradiance to the total irradiance for the horizontal surface. This ratio is dimensionless, ranges from 0 to 1, and maybe estimated hourly from the value of  $k_T$ . Here again, the irradiance values have been used to approximate hourly irradiation values. Hence,  $I_d/I$  became  $G_d/G$  in the following Equations [23]:

$$\frac{G_d}{G} = 1.0 - 0.249k_T \quad \text{for } k_T < 0.35 \quad (17)$$

$$\frac{G_d}{G} = 1.557 - 1.84k_T \quad \text{for } 0.35 < k_T < 0.75 \quad (18)$$

$$\frac{G_d}{G} = 0.177 \quad \text{for } k_T > 0.75 \quad (19)$$

### 3.3 Calculation Procedure

Figure 3.1 shows the detailed calculation procedure used in estimating the horizontal solar irradiance ( $G$ ) at each array by back calculating from the estimated solar irradiance on the tilted array ( $G_t$ ). The solar irradiance on the tilted arrays was earlier estimated in Chapter 2. In addition, the following are assumptions used in performing the calculations:

1. The atmosphere is standard with a visibility  $\geq 23$  km and an altitude (elevation) of  $\leq 2.5$  km.
2. Albedo ( $\rho_g$ ) or ground reflection is 0.9 on January 1 (ice and snow) while on May 26 and July 2 it is 0.7 and 0.2, respectively.

### 3.4 Albedo Analysis

A sensitivity analysis was performed to see the effect of varying the albedo by  $\pm 0.1$ , to determine if that would decrease the difference in  $G$  calculated from the two arrays.

### 3.5 Comparison to Historical Values

Isolation data for Iqaluit for the period 1953-2005 for the dates and times analyzed was extracted from the CWEEDS database [27]. Reported hourly horizontal irradiation values were converted to irradiance ( $G$ ) and averaged.

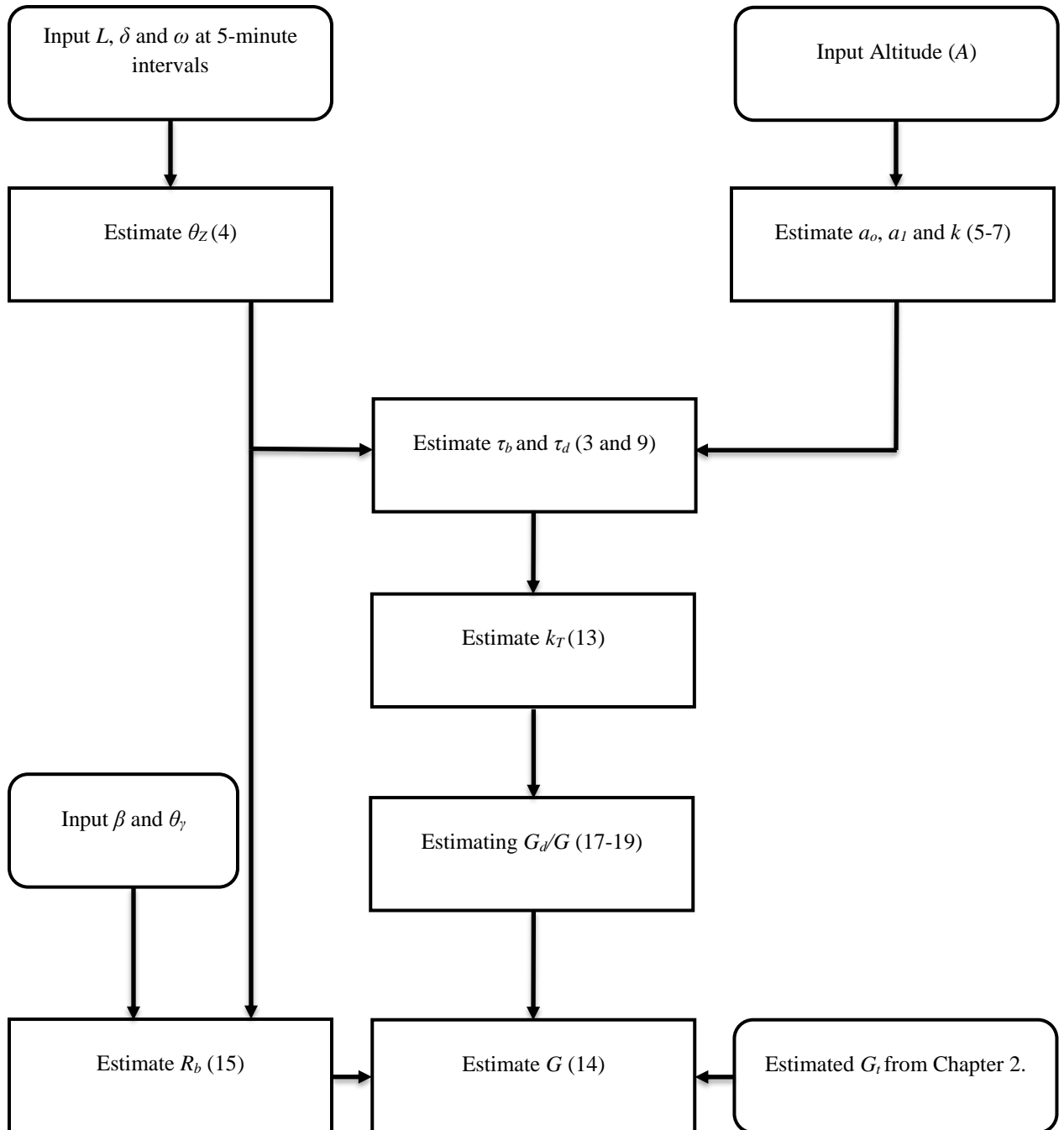


**Figure 3.1** Flow chart showing calculating of horizontal solar irradiance  $G$ . Numbers in brackets are relevant equations.

### 3.6 Results and Discussions

Figures 3.2, 3.3 and 3.4 shows a plot of the arrays' estimated horizontal solar irradiance ( $G$ ) versus estimated solar irradiance on the tilted array ( $G_t$ ) on clear and sunny winter, spring and summer days, respectively for the arrays at QEC and AWGA. The results showed that on all three days during the analysis period, the estimated horizontal solar irradiance ( $G$ ) at QEC differs significantly from the values estimated at AWGA. That is, on the winter day the average, estimated horizontal solar irradiance ( $G$ ) for the analysis period at QEC was  $11 \text{ W/m}^2$  while at AWGA it was  $3 \text{ W/m}^2$  for a difference of 114%. On the spring and summer days they were  $427 \text{ W/m}^2$  and  $450 \text{ W/m}^2$ , respectively at, QEC and at AWGA for the same period they were  $332 \text{ W/m}^2$  and  $315 \text{ W/m}^2$ , respectively. This gives a difference at the arrays locations of  $95 \text{ W/m}^2$  or 25% on the spring day while on the summer day it was  $135 \text{ W/m}^2$  or 35%.

In addition, Figures 3.2, 3.3 and 3.4 reveal that the difference of the horizontal solar irradiance ( $G$ ) is more significant in the afternoon: at AWGA, the curve starts to decline in the afternoon when compared to the curve at QEC. Since the distance between QEC and AWGA is only 2 km and they are at the same latitude and longitude, it was expected that the estimated values for the horizontal solar irradiance ( $G$ ) at both arrays would be the same. A possible reason for this difference in values at the locations may be due to shading of the arrays at AWGA by the building walls, roof and/or garage attachment. A brief shading analysis was then performed, selecting possible shading points on the building walls and rooves for both arrays (Appendix A) and calculating the solar altitude and azimuth angles that would lead to shading. University of Oregon sun-path software available online [28] was used to create sun-path charts for Iqaluit on the three days

examined. The calculated altitude and azimuth angles were plotted on the sun-path diagrams. The results from the shading analysis indicated that the array at QEC is not affected by shading for the period of analysis on any of three days. However, the same cannot be said for the array at AWGA, which is significantly affected by partial shading after approximately 12:45 hours on the winter, spring and summer days. The shading and no-shading period for both arrays are separated by vertical lines in Figures 2, 3 and 4. The analysis and sun-path diagrams may be found in Appendix B.

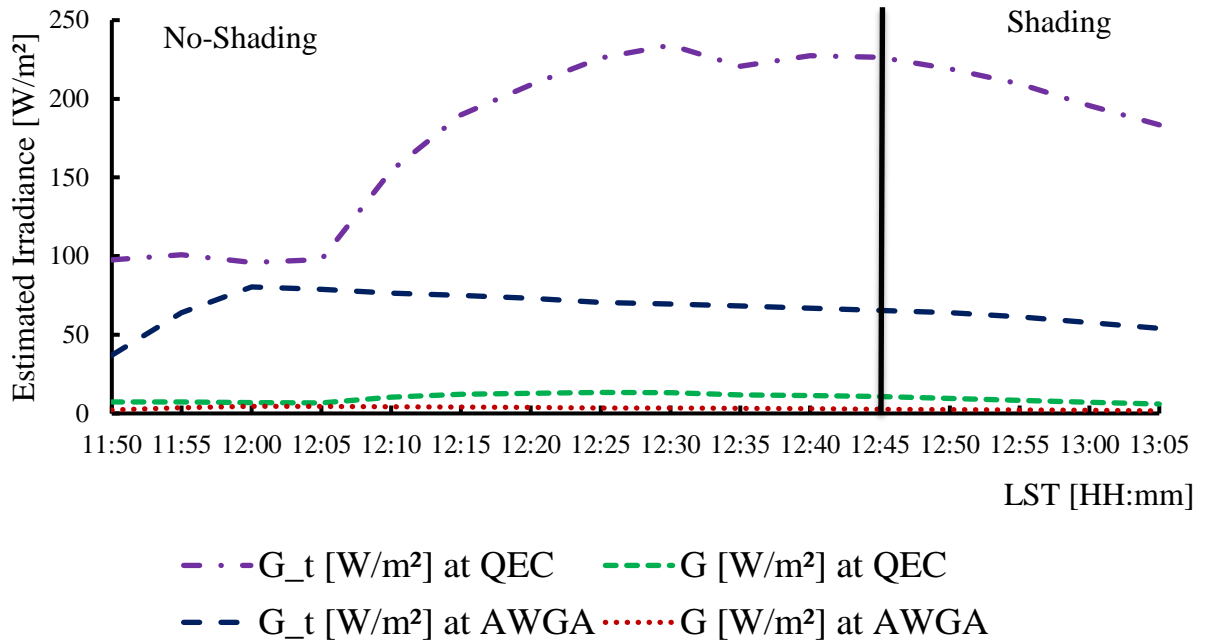


Figure 3.2 Estimated horizontal solar irradiance (G) for both arrays on January 1, 2017

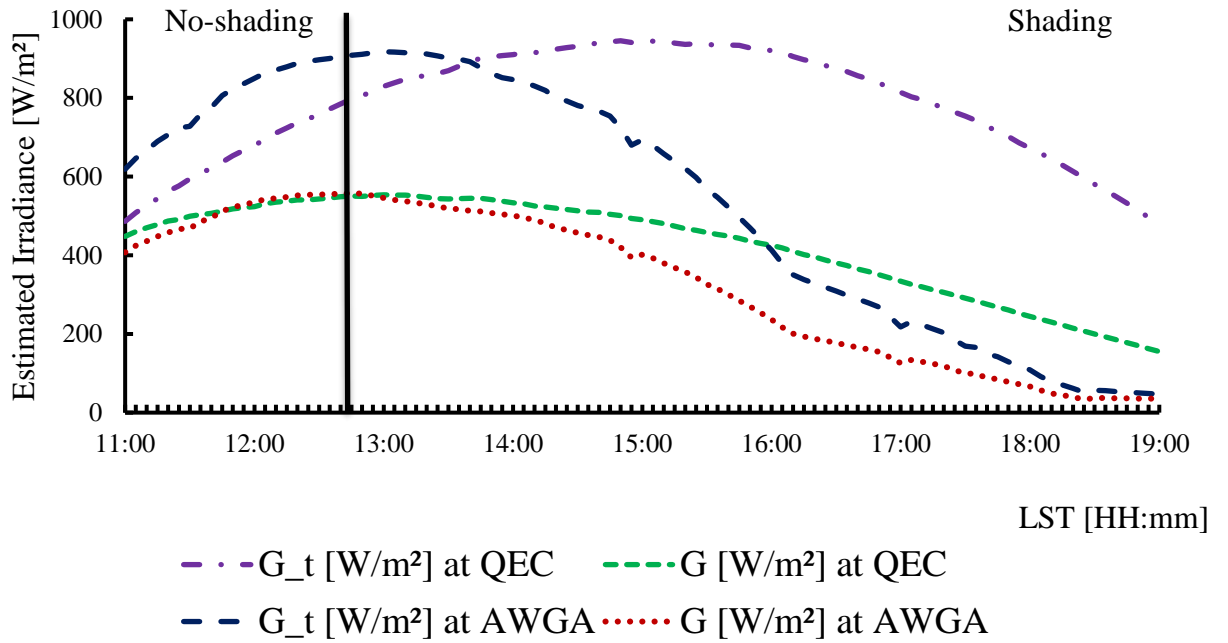


Figure 3.3 Estimated horizontal solar irradiance (G) for both arrays on May 26, 2017

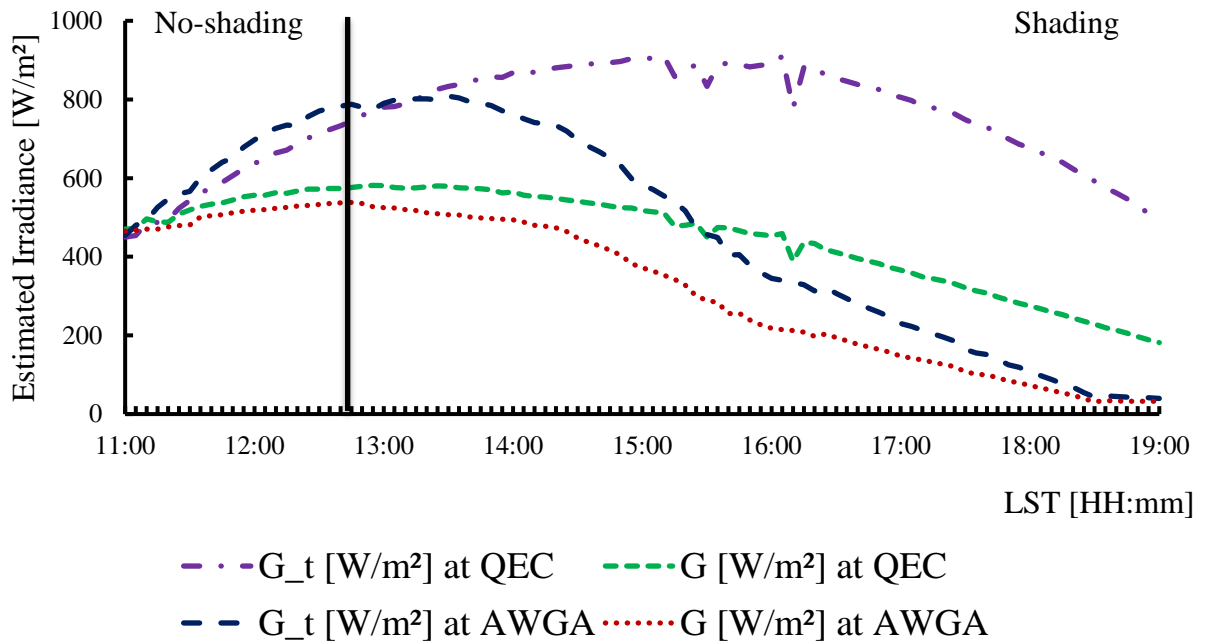


Figure 3.4 Estimated horizontal solar irradiance (G) for both arrays on July 2, 2017

Table 3.1 shows the comparison of the average estimated horizontal solar irradiance (G) at QEC to AWGA and their differences when only the no-shading period was taken in

account versus when shading was included. The no-shading analysis period on the winter day at both arrays was from 11:50 hours to about 12:45 hours while on the spring and summer days it was from 11:00 hour to about 12:45 hours. During the period of no-shading on the winter day at QEC, the average estimated horizontal solar irradiance ( $G$ ) was 10 W/m<sup>2</sup> while at AWGA it was 4 W/m<sup>2</sup> resulting in an average difference at the locations of 86%. For the spring and summer days at QEC they were 513 W/m<sup>2</sup> and 537 W/m<sup>2</sup>, respectively. While for the same period at AWGA, they were 507 W/m<sup>2</sup> and 509 W/m<sup>2</sup>, respectively. Thus, the average differences of the estimated horizontal solar irradiance ( $G$ ) for the spring and summer days were 6 W/m<sup>2</sup> or 1% and 28 W/m<sup>2</sup> or 5%, respectively. When comparing the whole analysis period of no-shading, the difference at both arrays decreased on all three days. That is, on the winter day it decreased from 114% to 86% while for the spring and summer days the difference decreased from 25% to 1% and 35% to 5%, respectively.

After analyzing the shading versus the no-shading period, it appears that shading is a major factor in the significant difference of the estimated horizontal solar irradiance ( $G$ ) values at the QEC and AWGA arrays.

**Table 3.1. Shows the average G at no-shading versus shading and differences during the analysis for both arrays.**

Analysis Period	QEC		AWGA		Differences			
	$\bar{G}_s$ [W/m <sup>2</sup> ]	$\bar{G}_{ns}$ [W/m <sup>2</sup> ]	$\bar{G}_s$ [W/m <sup>2</sup> ]	$\bar{G}_{ns}$ [W/m <sup>2</sup> ]	$\Delta\bar{G}_s$ [W/m <sup>2</sup> ]	$\Delta\bar{G}_s / \bar{G}_s$ [%]	$\Delta\bar{G}_{ns}$ [W/m <sup>2</sup> ]	$\Delta\bar{G}_{ns} / \bar{G}_{ns}$ [%]
<b>Jan.1</b>	<b>11</b>	<b>10</b>	<b>3</b>	<b>4</b>	<b>8</b>	<b>114</b>	<b>6</b>	<b>86</b>
<b>May 26</b>	<b>427</b>	<b>513</b>	<b>332</b>	<b>507</b>	<b>95</b>	<b>25</b>	<b>6</b>	<b>1</b>
<b>Jul. 2</b>	<b>450</b>	<b>537</b>	<b>315</b>	<b>509</b>	<b>135</b>	<b>35</b>	<b>28</b>	<b>5</b>

$\bar{G}_{ns}$  is the average estimated horizontal solar irradiance during no-shading period

$\bar{G}_s$  is the average estimated horizontal solar irradiance during the period with shading (that is for the entire analysis period).

$$\Delta\bar{G}_s \text{ [W/m}^2\text{]} = \bar{G}_{s, \text{QEC}} - \bar{G}_{s, \text{AWGA}}$$

$$\Delta\bar{G}_s / \bar{G}_s \text{ [%]} = \{(\bar{G}_{s, \text{QEC}} - \bar{G}_{s, \text{AWGA}}) / [(\bar{G}_{s, \text{QEC}} + \bar{G}_{s, \text{AWGA}}) / 2]\} \times 100$$

$$\Delta\bar{G}_{ns} \text{ [W/m}^2\text{]} = \bar{G}_{ns, \text{QEC}} - \bar{G}_{ns, \text{AWGA}}$$

$$\Delta\bar{G}_{ns} / \bar{G}_{ns} \text{ [%]} = \{(\bar{G}_{ns, \text{QEC}} - \bar{G}_{ns, \text{AWGA}}) / [(\bar{G}_{ns, \text{QEC}} + \bar{G}_{ns, \text{AWGA}}) / 2]\} \times 100$$

Figure 3.5 shows a plot of the calculated impact of ground reflection on both arrays' output ( $G_t$ ) during the no-shading analysis period. The day when the albedo mostly impacted the arrays' output was the clear and sunny spring day. On this day ground reflection accounted for an average of 105 W/m<sup>2</sup> of the solar irradiance on the plane ( $G_t$ ) of the array at QEC while at AWGA for the same period it was 81 W/m<sup>2</sup>. This represents 17% and 15% of the total irradiance on the titled arrays at QEC and AWGA, respectively. On the winter and summer days the averages of the reflected irradiances were approximately 13 W/m<sup>2</sup> and 22 W/m<sup>2</sup> at QEC, respectively. At AWGA for the same period, the average values were 5 W/m<sup>2</sup> and 16 W/m<sup>2</sup>, respectively. On the winter day this represents 7% and 8% of the total irradiance on the tilted array at QEC and AWGA, respectively while for the summer day it represents 4% and 5% at QEC and AWGA, respectively.

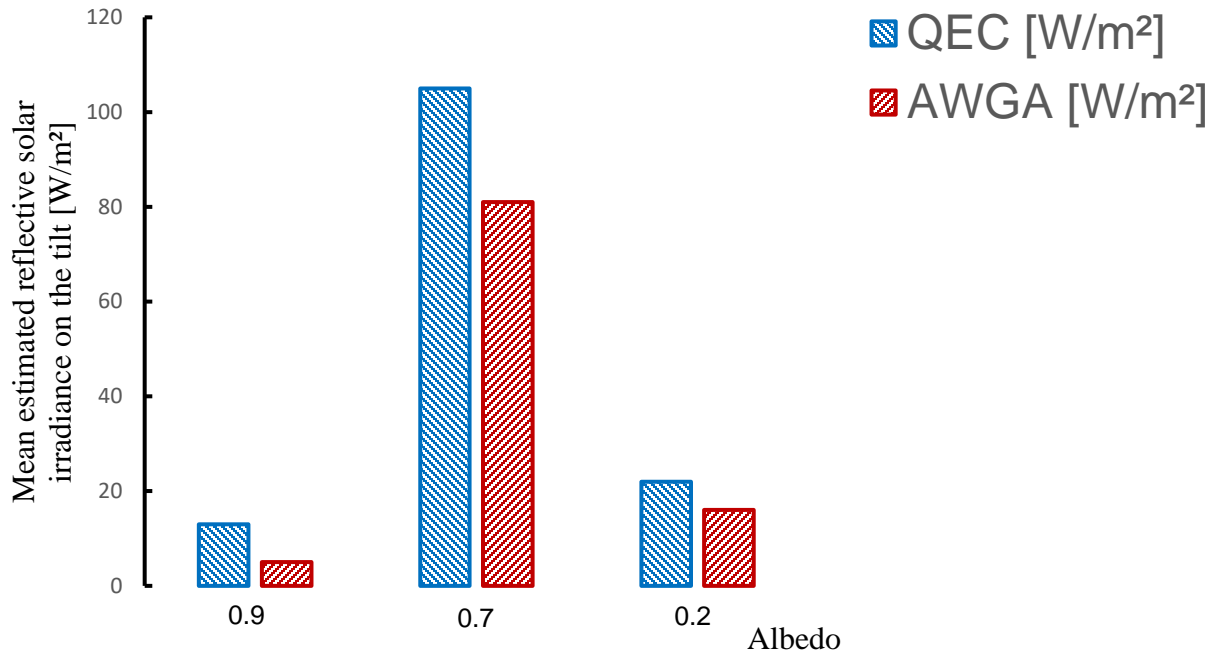


**Figure 3.5 Albedo impact during the analysis period at QEC and AWGA**

In addition, a test was done by changing the ground reflection values on the winter, spring and summer days by decreasing and increasing the assumed albedo at an increment of 0.1 to determine the impact of the ground reflection on the estimated horizontal solar irradiance ( $G$ ). Table 3.2 shows the average estimated horizontal solar irradiance ( $G$ ) and differences based on the different values of the albedo for the winter, spring and summer days during the period when both arrays were not shaded ( $\bar{G}_{ns, QEC}$  and  $\bar{G}_{ns, AWGA}$ ). For the winter day, when the albedo value was increased to 1.0 and decreased to 0.8, the average estimated horizontal solar irradiance ( $G$ ) remains unchanged as was initially estimated when the ground reflection was assumed at 0.9 at both QEC and AWGA. On the spring day when the albedo was increased to 0.8, the average estimated horizontal solar irradiance ( $G$ ) decreased to 495 W/m<sup>2</sup> and 476 W/m<sup>2</sup> at QEC and AWGA, respectively, resulting in an average difference of 4% between the two arrays. When the albedo was reduced to 0.6, the average estimated solar irradiance ( $G$ ) increased

to 517 W/m<sup>2</sup> and 509 W/m<sup>2</sup> at QEC and AWGA, respectively, resulting in an average difference of 2%. Neither of these is lower than the 1% difference resulting from using the original albedo of 0.7. For the summer day when the albedo were increased to 0.3, the average estimated horizontal solar irradiance ( $G$ ) decreased to 534 W/m<sup>2</sup> and 499 W/m<sup>2</sup> at QEC and AWGA, respectively, resulting in an average difference between arrays of 7%. Similarly, when the albedo was reduced to 0.1 the average estimated horizontal solar irradiance ( $G$ ) increased to 544 W/m<sup>2</sup> and 514 W/m<sup>2</sup> at QEC and AWGA, respectively, resulting in an average difference between arrays of 6%. Again, these differences are higher than the differences obtained when using an albedo of 0.2. Hence, the results obtained from increasing and decreasing the albedo compared to the original albedo values were poorer.

Lower average differences ( $\Delta G$ ) between QEC and AWGA means that the initial values used in estimating the horizontal solar irradiance ( $G$ ) was more accurate, that is leading to a more similar values of horizontal solar irradiance ( $G$ ) for the two arrays.

**Table 3.2 Shows the average  $G$  and differences as the ground reflection varies for both arrays**

Season	$\rho_g$	$\bar{G}_{ns, QEC}$ [W/m <sup>2</sup> ]	$\bar{G}_{ns, AWGA}$ [W/m <sup>2</sup> ]	$\Delta \bar{G}_{ns} / \bar{G}_{ns}$ [%]
Winter	1.0	10	4	86
	0.9	10	4	86
	0.8	10	4	86
Spring	0.8	495	476	4
	0.7	513	507	1
	0.6	517	509	2
Summer	0.3	534	499	7
	0.2	537	509	5
	0.1	544	514	6

Table 3.3 shows the estimated values of  $G$  compared to historic values. The winter  $G$  values at QEC and AWGA were lower than historic values, whereas the spring and summer values at QEC and AWGA were higher than historic averages.

**Table 3.3 Shows the estimated values of  $G$  compared to historic values and standard deviation**

Analysis Period	$\bar{G}_{ns, QEC}$ [W/m <sup>2</sup> ]	$\bar{G}_{ns, AWGA}$ [W/m <sup>2</sup> ]	Historical [W/m <sup>2</sup> ] (Standard Deviation)
January 1	10	4	21 (14)
May 26	513	507	503 (7)
July 2	537	509	487 (36)

Notably, the summer value is 1.4 standard deviations above the mean for QEC and 0.6 standard deviations above the mean for AWGA. Further analysis could reveal whether the higher-than historic spring and summer values represent an overall increase in intensity of the solar irradiance with time. The difference could also be caused by:

1. Inaccuracy in using PV output values as a way to measure  $G$ .
2. Random weather. 2017 may just be a “sunny year” compared to the average.

### 3.7 Conclusion

These analyses estimated the solar horizontal irradiance ( $G$ ) at two PV arrays in Arctic conditions on clear and sunny days in winter, spring and summer of 2017, based on the array power outputs and using geometry and solar energy mathematical concepts. When the period of shading was excluded from the analysis, the difference in predicted horizontal solar irradiance for the two arrays was 6 W/m<sup>2</sup> or 86% for the winter day while for the

spring and summer days, the values were 6 W/m<sup>2</sup> or 1% and 28 W/m<sup>2</sup> or 5%, respectively. Comparing the whole analysis period to the no-shading period, saw a drop in the average difference on all three days with the most significant impact taking place on the spring and summer days.

In addition, changing the albedo when the period of shading was excluded from the analysis did not significantly impact the difference in predicted horizontal solar irradiance for the two arrays. On the winter day, the values remain unchanged compared to those calculated with an albedo of 0.9. On the spring and summer days the difference in values fluctuated but in all instances were greater than those calculated with the initial albedo. That is, on the spring day when the albedo were set to 0.8 and 0.6, the average difference was 4% and 2%, respectively, compared to 1% at 0.7. For the summer day when the albedo were set to 0.3 and 0.1, the average differences were 7% and 6%, respectively, compared to 5% at 0.2. When compared to historic irradiations values from 1953-2005, the solar isolation values found by back-calculating from PV array output were lower than the 53-year averages in the winter, but higher in the spring and summer.

It is recommended that the findings from this research be applied to a larger data set, or a case where the orientations of the arrays (tilt and azimuth) are more different than each other, or to a case where monitoring data from pyranometers is available in order to confirm the usefulness and applicability of this method. If found to be robust, this method can be used by future PV designers and developers where measured solar irradiance values are not readily available due to high costs.

## REFERENCES

- [1] S. Kalogirou, Solar Energy Engineering, in: Processes and Systems, Elsevier Inc., Burlington, MA, 2009.
- [2] L. Yang, X. Gao, F. Lv, X. Hui, L. Ma, X. Hou, Study on the local climatic effects of large photovoltaic solar farms in desert areas, *Solar Energy* 144 (2017) 244–253.
- [3] R. Singh, M. Sharma, C. Banerjee, C, Field analysis of three different Silicon-based technologies in composite climatic condition. *Solar Energy* 182 (2019) 102-116.
- [4] C. Brunet, O. Savadogo, P. Baptiste, M.A, Bouchard, Shedding some light on photovoltaic solar energy in Africa – A literature review, *Renewable and Sustainable Energy Reviews* 96 (2018) 325-342.
- [5] M. Bayrakci, Y. Choi, J.R.S Brownson, Temperature dependent power modeling of photovoltaics, *Energy Procedia* 57 (2014) 745–754.
- [6] M. Habibollahi, M. Ameri, S.H. Mansouri, Efficiency improvement of photovoltaic water pumping systems by means of water flow beneath photovoltaic cells surface, *Journal of Solar Energy Engineering* 137-4 (2015) 044501.
- [7] T. Ma, W. Gu, L. Shen, L, M. Li, An improved and comprehensive mathematical model for solar photovoltaic modules under real operating conditions, *Solar Energy* 184 (2019) 292–304.
- [8] J.C. Solano, M. C. Brito, E. Caamaño-Martín, Impact of fixed charges on the viability of self-consumption photovoltaics, *Energy Policy* 122 (2018) 322-331.

- [9] J. Al-Saqlawi, K. Madani, N. Mac Dowell, Techno-economic feasibility of grid-independent residential roof-top solar PV systems in Muscat, Oman. *Energy Conversion and Management* 178 (2018) 322-334.
- [10] Bayrakci, M., Choi, Y., & Brownson, J. R. S, Temperature dependent power modeling of photovoltaics. *Energy Procedia* 57 (2014) 745- 754.
- [11] K. Earley, Why renewables are winning the ‘carbon war’, *Renewable Energy Focus* 19-20 (2017) 117-120.
- [12] S. Jamali, A. Nemat, F. Mohammadkhani, M. Yari, Thermal and economic assessment of a solar chimney cooled semi-transparent photovoltaic (STPV) power plant in different climates, *Solar Energy* 185 (2019) 480-493.
- [13] P. Alamdari, O. Nematollahi, A.A. Alemrajabi, Solar energy potentials in Iran: A review, *Renewable and Sustainable Energy Reviews* 21 (2013) 778-788.
- [14] O. Ellabban, H. Abu-Rub, F. Blaabjerg, Renewable energy resources: Current status, future prospects and their enabling technology, *Renewable and Sustainable Energy Reviews* 39 (2014) 748-764.
- [15] J. M. Pearce, S.V. Obydenkova, Technical viability of mobile solar photovoltaic systems for indigenous nomadic communities in northern latitudes, *Renewable Energy* 89 (2016) 253–267.

- [16] L. Dignard-Bailey, S. Martel, M.M.D. Ross, Photovoltaics for the North: A Canadian Program, 2nd World Conference and Exhibition on Photovoltaic Solar Energy Conversion Vienna, Austria (1998).
- [17] B. Marion, B. Smith, Photovoltaic system derived data for determining the solar resource and for modeling the performance of other photovoltaic systems, Solar Energy 147 (2017) 349-357.
- [18] E. Paulescu, R. Blaga, A simple and reliable empirical model with two predictors for estimating 1-minute diffuse fraction, Solar Energy 180 (2019) 75-84.
- [19] S. A. M Maleki, H. Hizam, C. Gomes, Estimation of hourly, daily and monthly global solar radiation on inclined surfaces: Models re-visited, Energies (2017).
- [20] R. Djebbar, Solar Resource Assessment in Canada, Natural Resources Canada – CanmetENERGY (2011).
- [21] Latitude, Iqaluit Nunavut Canada Latitude. <http://latitude.to/articles-by-country/ca/canada/1534/iqaluit>, (accessed 7 May, 2018).
- [22] S. A. M Maleki, H. Hizam, C. Gomes, Estimation of hourly, daily and monthly global solar radiation on inclined surfaces: Models re-visited, Energies (2017).
- [23] J.A. Duffie, W. A. Beckman, W. A., Solar Engineering of Thermal Processes, second ed., John Wiley and Sons, New York, 1980.

- [24] H.C. Hottel, A simple model for estimating the transmittance of direct solar radiation through clear atmospheres, *Solar Energy* 18-2 (1976) 129-134.
- [25] B.Y.H. Liu, R.C. Jordan, The interrelationship and characteristic distribution of direct, diffuse and total solar radiation, *Solar Energy* 4-3 (1960) 1-19.
- [26] J.F. Orgill, K.G.T. Hollands, Correlation equation for hourly diffuse radiation on a horizontal surface, *Solar Energy* 19-4 (1977) 357-359.
- [27] Environment Canada, Canadian Weather Energy and Engineering Datasets (CWEEDS). [https://climate.weather.gc.ca/prods\\_servs/engineering\\_e.html](https://climate.weather.gc.ca/prods_servs/engineering_e.html), (accessed 15 February, 2018).
- [28] Sun Path Chart Program, University of Oregon.  
<http://solardat.uoregon.edu/SunChartProgram.html>, (accessed 29 November, 2019).

## CHAPTER 4

### CONCLUSIONS AND RECOMMENDATIONS

#### 4.1 Summary and Conclusion

In Chapter 2, two separate solar PV arrays located in Iqaluit, Canada were analyzed to estimate each array's output electrical efficiency. The arrays efficiencies were estimated from the arrays power output data measured by the inverters and manufacturers' reference efficiencies, modified by the effects of ambient temperature and wind. Further analysis was performed to understand the heat loss mechanisms at various times of the year. Sensitivity of the energy balance to the use of different equations describing the convective heat loss coefficient, sky temperature and view factors was examined. The annual mean relative enhancement in efficiency was calculated.

Based on the estimated results it was found that both arrays are performing above their rated capacity by 4% to 7% on a mean annual energy-weighted basis. During the winter days radiation to the sky was the dominant heat loss mode in cooling of the PV cells while during the other seasons, convection to the ambient air was the dominant heat loss mode. In addition, calculating the heat loss from the PV array, it was found that the Test et al. convection heat transfer coefficient model, the Swinbank sky temperature model, and the Armstrong and Hurley view factors provided the least error in the energy balance. The lower error gives more confidence that all significant heat losses were considered,

In Chapter 3, two separate solar PV arrays located in Iqaluit, Canada were analyzed to estimate the solar horizontal irradiance ( $G$ ). The horizontal solar irradiance were calculated in two phases. Firstly, the values of solar irradiance on the tilted array

( $G_t$ ) from Chapter 2 were used to back-calculate the horizontal solar irradiance ( $G$ ). The array at Qulliq Energy Corporation (QEC) during the analysis period was not affected by shading while the array at Arctic Winter Game Arena (AWGA) was experiencing partial shading after about 12:45 hours on clear and sunny winter, spring and summer days. During the period when the array at AWGA was affected by shading and the array at QEC was not, the average difference in predicting the horizontal solar irradiance ( $G$ ) within the arrays was 114% on the winter day while on the spring and summer days it was 25% and 35%, respectively. Hence, during the period when both arrays were not affected by the shading, the average difference reduced from 114% to 86% on the winter day while for the spring and summer days the difference was reduced from 25% to 1% and 35% to 5%, respectively. Analysis further reveals that the ground reflection had a greater impact on both arrays output on the spring day when compared to the winter and summer days. On the spring day, the ground reflected irradiance was 15% at QEC while at AWGA it was 17% of the total irradiance on the arrays when the albedo was assumed at 0.7. The estimated of  $G$  values from  $G_t$  values was not improved by varying the albedo from 0.9, 0.7 and 0.2 in the winter, spring and summer, respectively. Compared to 53 years at historic data there estimates of  $G$  were slightly low in the winter and high in the spring. In the summer the values were well over the historic means.

Below are a summary of the contribution of this thesis to the solar PV research area:

1. The 4% to 7% annual enhancement in power output of PV arrays shows the effect of cooling of the solar arrays resulting from radiation to sky and convection to ambient air heat loss modes. On the winter day, radiation to the sky was dominant

heat loss mode in cooling of PV arrays when compared to convection to ambient air. However, for the spring and summer days it was the opposite, that is, the convection to the ambient air was more dominant heat loss mode. The effect of cooling by wind was negligible.

2. During the analysis period, the ground-reflected solar radiation was highest on the spring day compared to the winter and summer days. The standard albedo values of 0.9 for winter, 0.7 for spring and 0.2 for summer gave the best results.
3. The average horizontal solar irradiance ( $G$ ) at the arrays location was estimated to be lower than that of the 1953-2005 historical values for the winter day while for the spring and summer days the average estimated values were higher than the historical values.

In addition, during the analysis of estimating the effect of cooling on the PV arrays and the back-calculation of the horizontal solar irradiance ( $G$ ), the research and its applicability are limited to:

- Isotropic model used to convert horizontal to the plane-of-the-array irradiance.
- Linear relationship between cell temperature ( $T_c$ ) and the array performance efficiency based on outdoor ambient temperature and wind velocity.
- Days chosen are typically clear and sunny.
- PV array inverter and other conditioning losses are negligible.
- $G_d/G = I_d/I$  used to estimate irradiance values.

## 4.2 Recommendations

Based on the results obtained from the research it is highly likely that there is an enhancement in PV output, which requires better data quantification. Hence, it is recommended that future researchers:

1. Analyze data for the identical days in the research for years other than 2017.

In addition, the analysis should take into consideration an uncertainty of the values and compare the results statistically against historical data. This will better quantify and confirm the main drivers in enhancing performance.

2. Procure and install field instruments to measure the total horizontal solar irradiance ( $G$ ) and diffuse horizontal solar irradiance at the site. With the installation of field measuring instrument at the site to measure  $G$ , the estimated results from back-calculation can be compared to the measured data, thus, this will determine how robust is the method in Chapter 3.

If found to be robust, then the method can be used to adjust historical solar irradiance data based on output from PV arrays in sub-arctic climate locations to estimate  $G$  where pyranometers are unavailable. These adjustments are important to PV designers in optimizing the components of their systems.

## APPENDICES

### APPENDIX A: SOLAR PV ARRAYS AND SPECIFICATIONS

Figures A1 and A2 show pictures of the Solar PV arrays at QEC and AWGA, respectively. The specifications of the arrays are as follows:

**Table 1A Array Specifications**

Description	Unit	Array Specifications	
		QEC	AWGA
Number of Panels (No.)	No.	11	40
Rated Power Output ( $P_o$ )	kW	2.8	10.0
Array Area	m <sup>2</sup>	18.0	64.34
Rated Array Efficiency ( $\eta_R$ )	%	15.89	16.16
Array Tilt ( $\beta$ )	Degrees	60	60
Array Azimuth ( $\gamma$ )	Degrees	45	11.3
Array Distance Apart	km	2	



**Figure A1 Southern View of Array at QEC (Letters and numbers represents shading points)**

**[Source: Green Sun Rising Incorporated]**

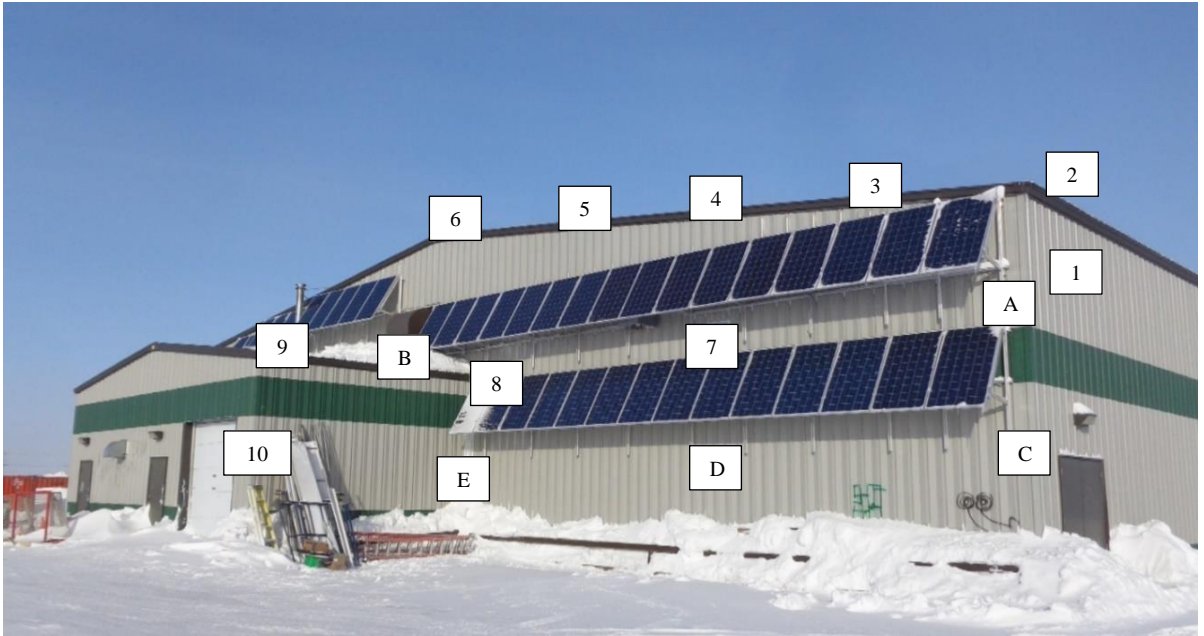


**Figure A2 Southeastern View of Array at AWGA (Letters and numbers represents shading points)**

**[Source: Green Sun Rising Incorporated]**

## APPENDIX B: SUN PATH AND SHADING ANALYSIS

Figures B1, B2, B3, B4, B5, B6, B7, B8 and B9 show the sun path from sunrise to sunset and that of the estimated shading angles for the arrays at QEC and AWGA, respectively, during the analysis period. In order to analyze shading of the arrays during the sun path from sunrise to sunset, possible shading surfaces and points were identified and labelled with letters and numbers as shown in Figures A1 and A2. The letters represented the array surface potentially being shaded while the numbers represented the points creating the shading onto the array surface. Then, the altitude and azimuth angles formed between each letter-number pair in figures A1 and A2 was determined by geometry and plotted on the sun path diagram for the various days. From the plots, both arrays are having restriction of sunlight due to shading on all three days. On the winter day selected, the sun path was from  $150^{\circ}$  or 10 am to  $210^{\circ}$  or 2 pm. Hence, the array at QEC sees no shading restriction since the restrictions are outside of the sun path while at the AWGA there is shading restriction commencing at about 12:45 pm. For the clear and sunny spring and summer days, the sun path was from  $30^{\circ}$  or 2 am to  $330^{\circ}$  or 10 pm. However, on these days the array at QEC is considered to not be affected by the shading restrictions since the data that was analyzed for those days were taken from  $150^{\circ}$  or 10 am to  $285^{\circ}$  or 7 pm on May 26 and  $165^{\circ}$  or 11 am to  $285^{\circ}$  or 7 pm on July 2. During this time, the shading restriction was outside of the analysis period. At AWGA for the same period there is shading restriction commencing at about  $191.3^{\circ}$  or 12:45 pm. See Chapters 2 and 3 for explanation why the complete sets of data were not used for analysis on the mentioned days.

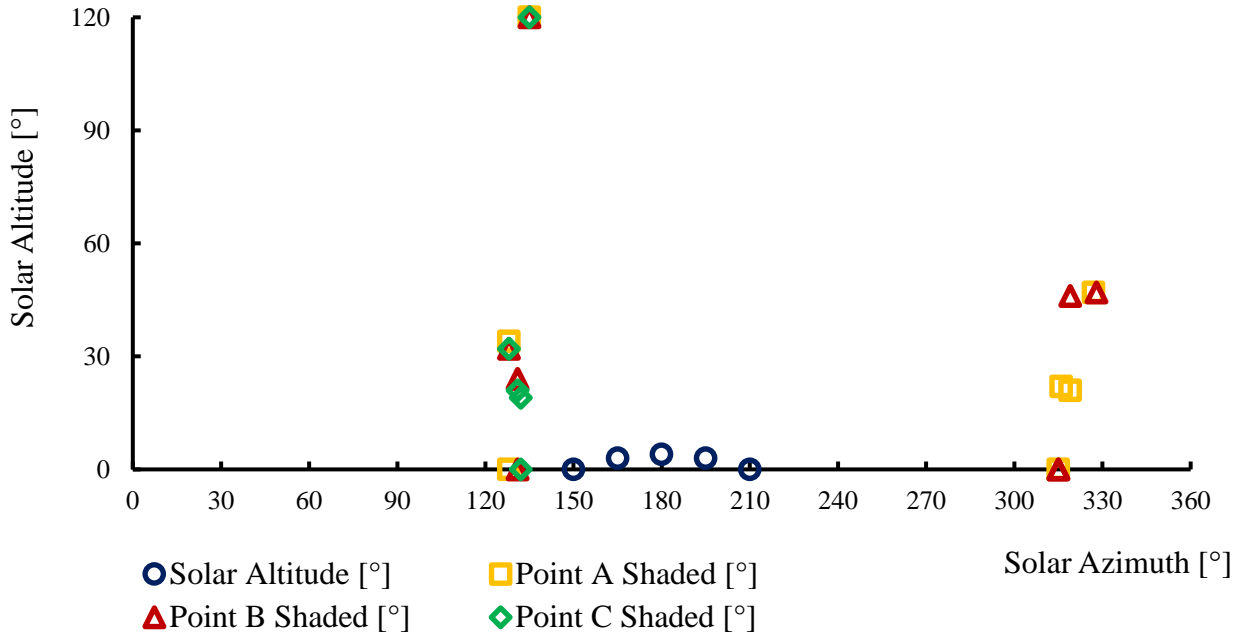


Figure B1 Sun path and array shading at QEC for January 1, 2017

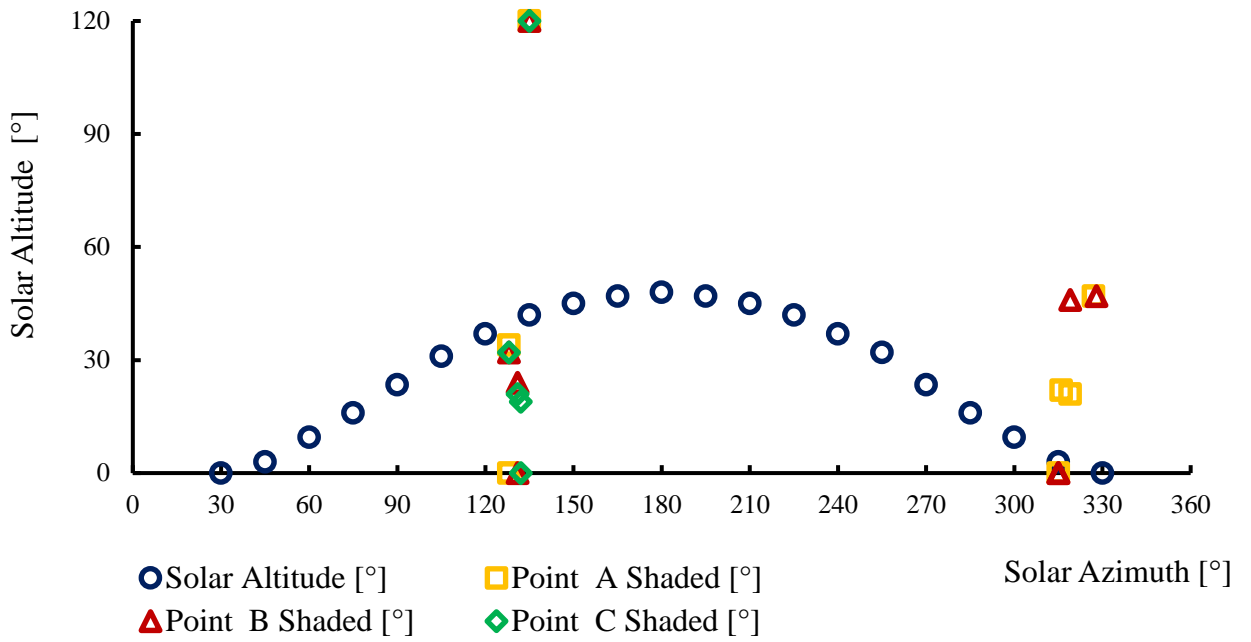


Figure B2 Sun path and array shading at QEC for May 26, 2017

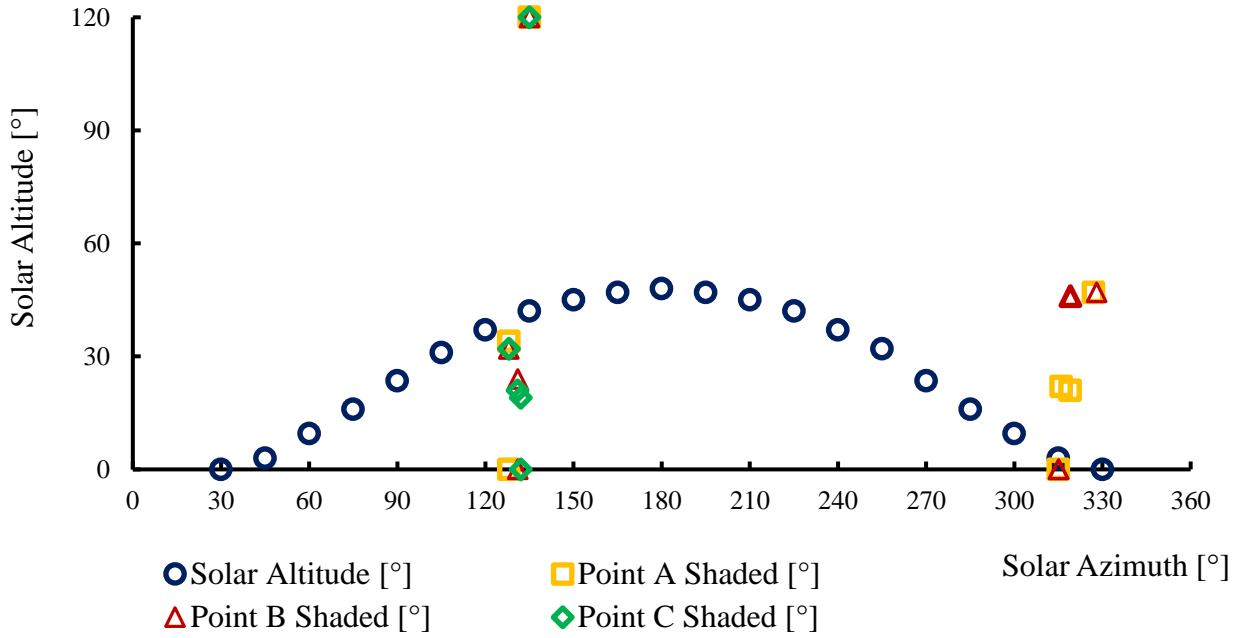


Figure B3 Sun path and array shading at QEC for July 2, 2017

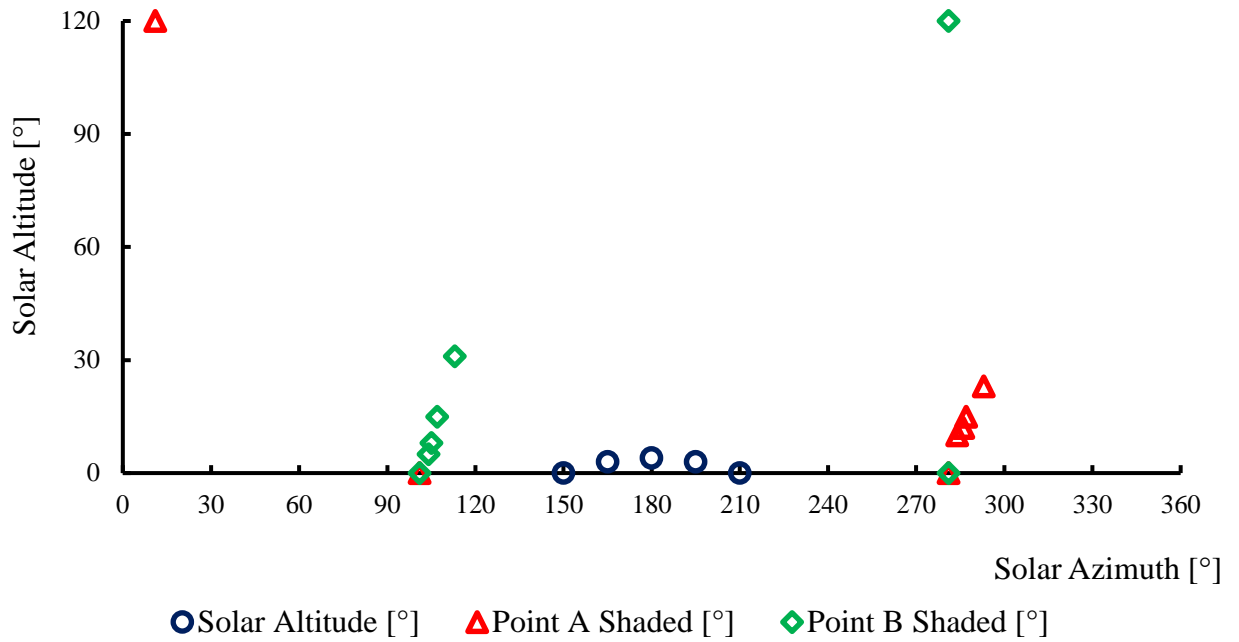


Figure B4 Sun path and top array shading at AWGA for January 1, 2017

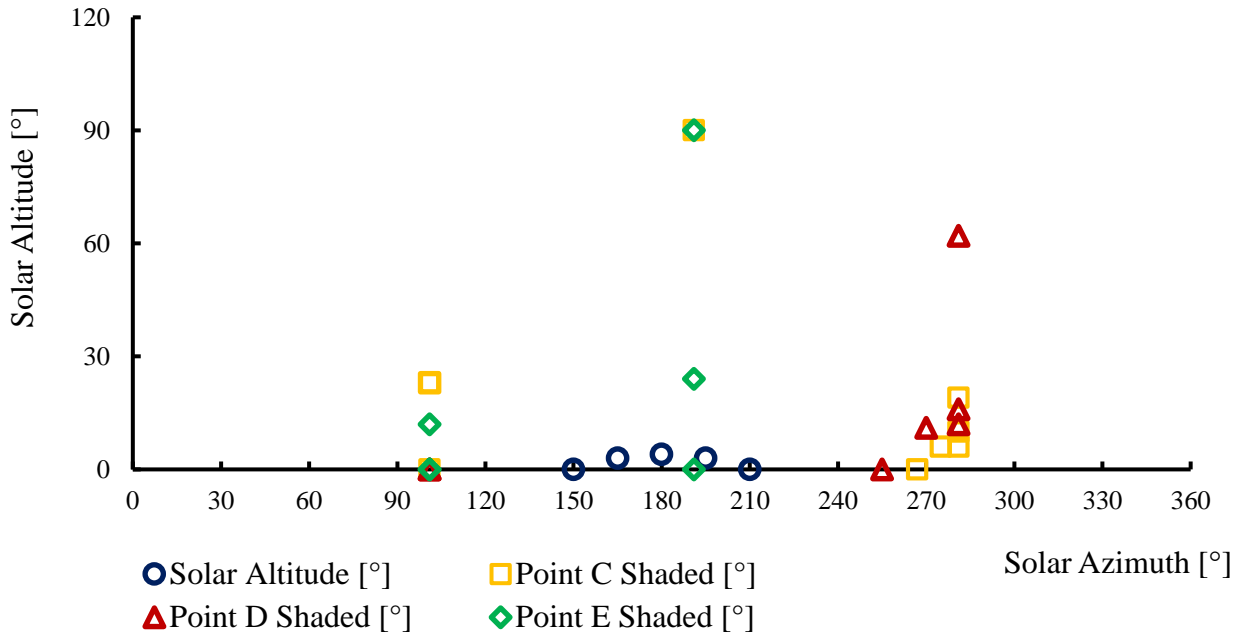


Figure B5 Sun path and bottom array shading at AWGA for January 1, 2017

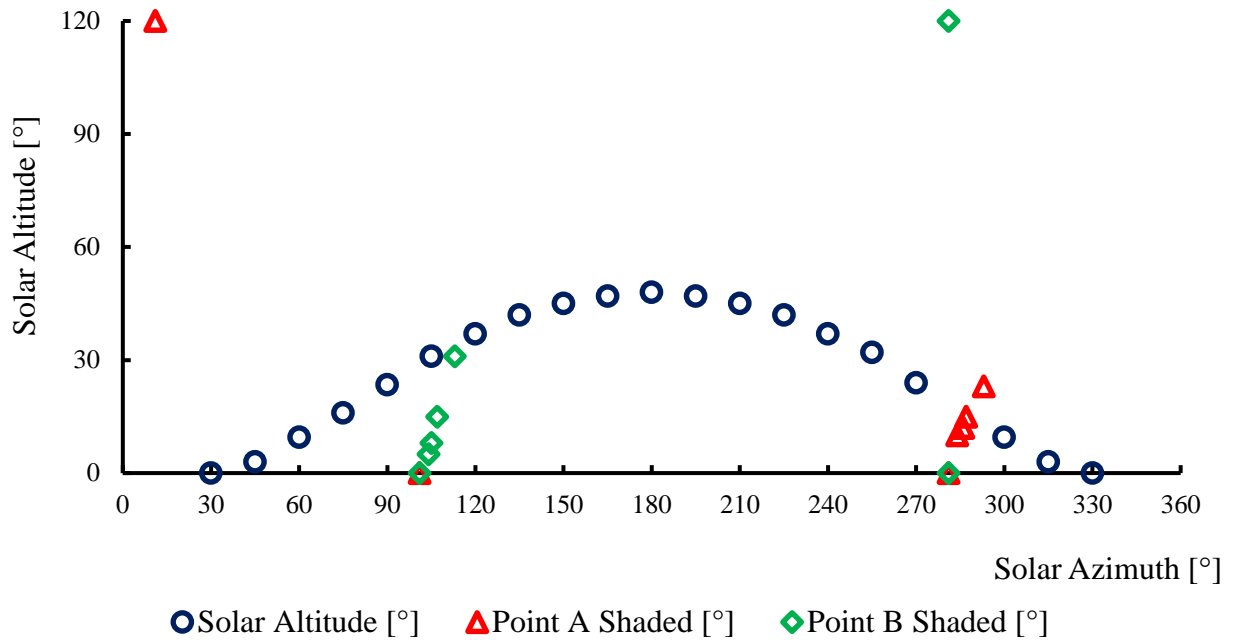


Figure B6 Sun path and top array shading at AWGA for May 26, 2017

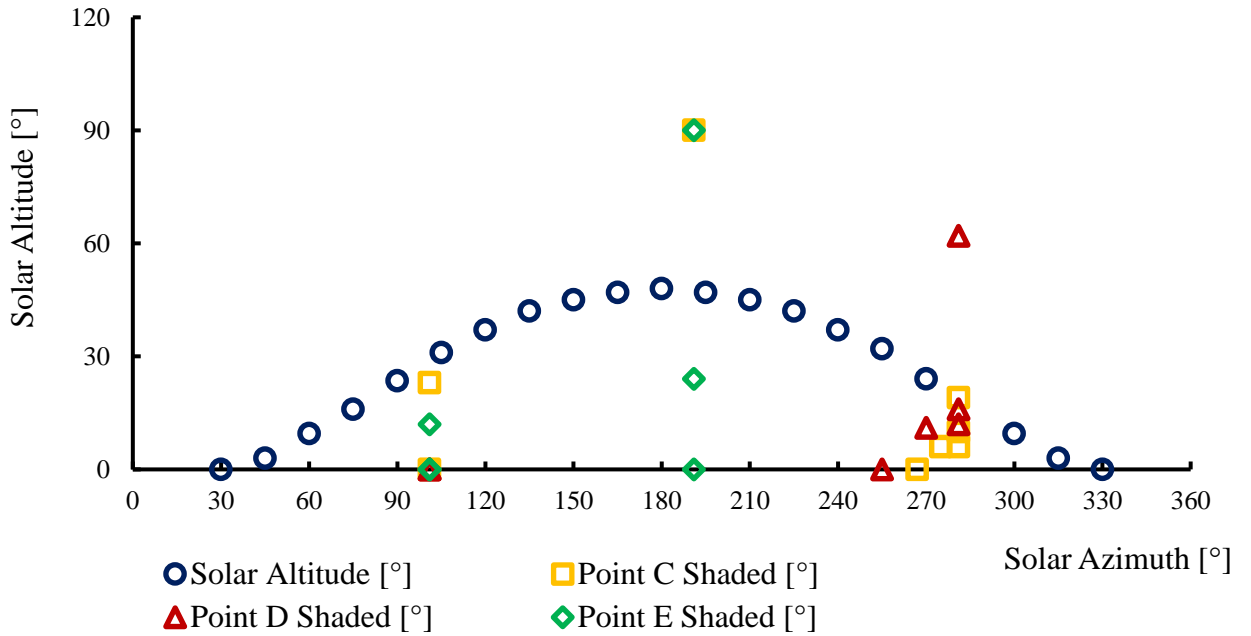


Figure B7 Sun path and bottom array shading at AWGA for May 26, 2017

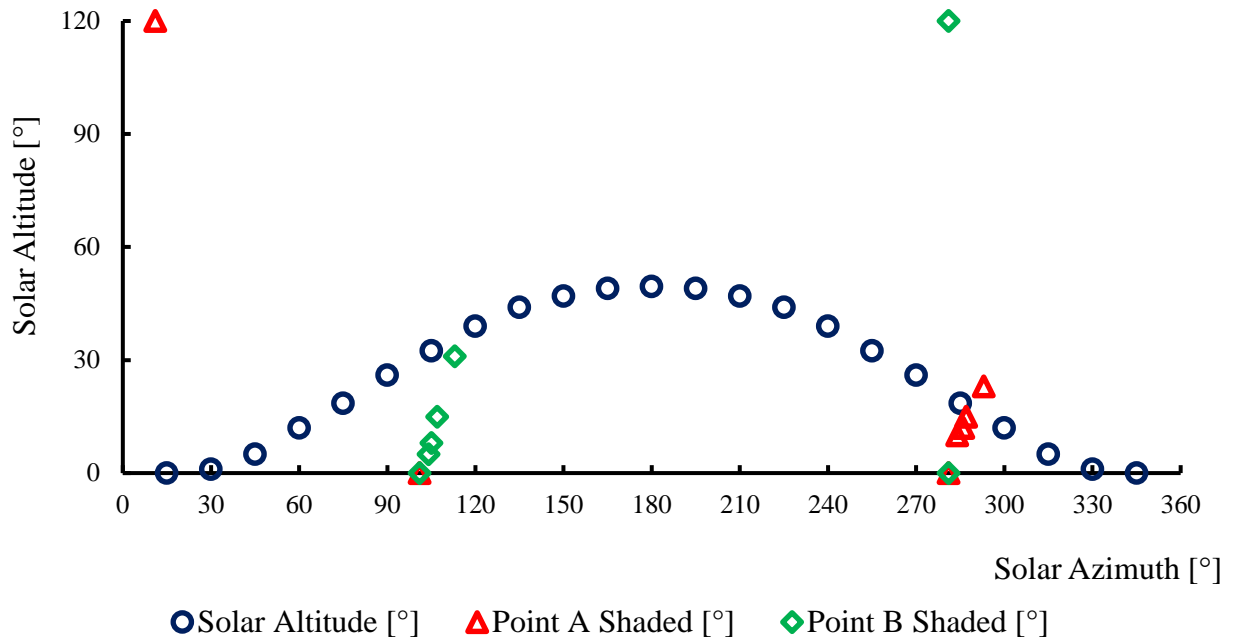


Figure B8 Sun path and top array shading at AWGA for July 2, 2017

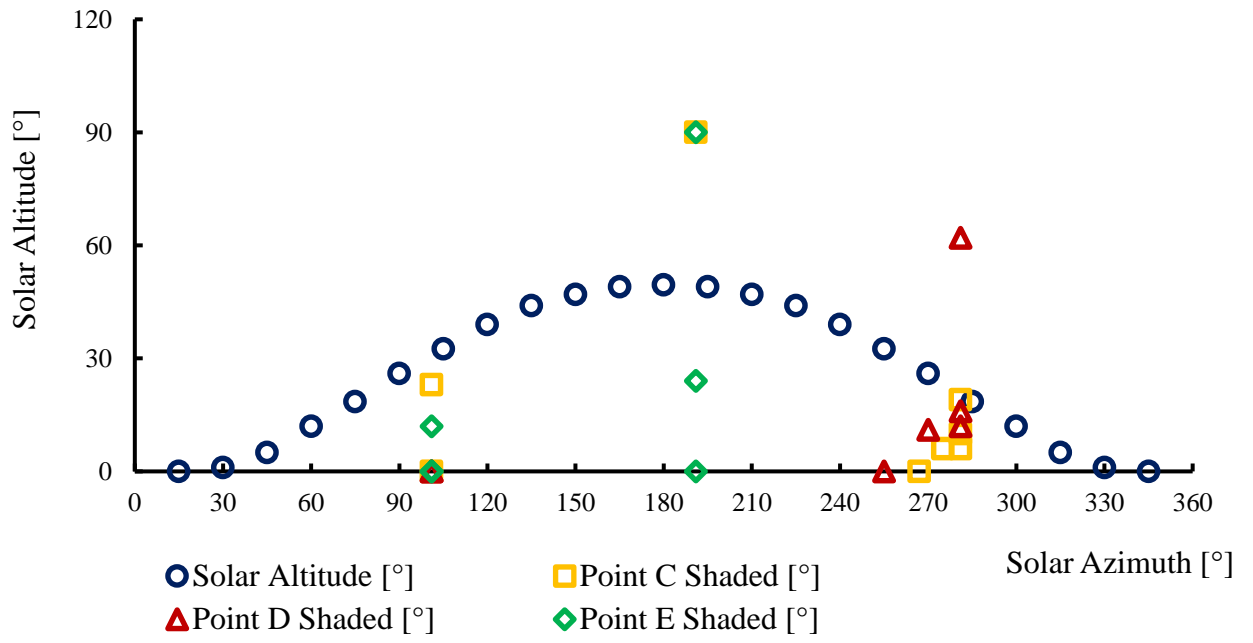


Figure B9 Sun path and bottom array shading at AWGA for July 2, 2017

**APPENDIX C: ESTIMATING THE HORIZONTAL SOLAR IRRADIANCE (G)  
USING A SIMULTANEOUS SOLUTION METHOD**

In theory, the horizontal solar irradiance ( $G$ ) can be calculated from multiple arrays at the same location, which have a different tilt ( $\beta$ ) and/or azimuth ( $\gamma$ ). This is a proxy method to determine  $G$  when pyranometers are not available. This method was applied to two arrays: QEC (array 1) and AWGA (array 2) as describing in the following pages:

The equation relating horizontal solar irradiance ( $G$ ) to solar irradiance on a tilted surface ( $G_t$ ) for array 1 is:

$$G_{t1} = G_1 \left\{ R_{b1} \left[ 1 - \frac{G_{d1}}{G_1} \right] + \left( \frac{G_{d1}}{G_1} \right) \left[ \frac{1+\cos\beta_1}{2} \right] + \rho_g \left[ \frac{1-\cos\beta_1}{2} \right] \right\} \quad (C1)$$

Where  $R_{b1}$  and  $G_{d1}/G_1$  are the beam radiation tilt factor and a characteristic of the sky clearness.

$$R_{b1} = \frac{\cos\theta}{\cos\theta_z} \quad (C2)$$

Expanding and simplifying equation gives

$$G_{t1} = G_1 \left\{ R_{b1} - R_{b1} \left( \frac{G_{d1}}{G_1} \right) + \frac{G_{D1}}{G_1} \left[ \frac{1+\cos\beta_1}{2} \right] + \rho_g \left[ \frac{1-\cos\beta_1}{2} \right] \right\} \quad (C3)$$

$$G_{t1} = G_1 \left\{ R_{b1} + \rho_g \left[ \frac{1-\cos\beta_1}{2} \right] + \left( \frac{G_{D1}}{G_1} \right) \left[ \frac{1+\cos\beta_1}{2} - R_{b1} \right] \right\} \quad (C4)$$

Let

$$a_1 = R_{b1} + \rho_g \left[ \frac{1-\cos\beta_1}{2} \right] \quad (C5)$$

$$b_1 = \left( \frac{1+\cos\beta_1}{2} - R_{b1} \right) \quad (C6)$$

Then Equation for Array 1: QEC becomes

$$G_1 = \frac{G_{t1}}{a_1 + \left(\frac{G_{d1}}{G_1}\right)b_1} \quad (C7)$$

### Array 2: AWGA

The equation relating horizontal solar irradiance ( $G$ ) to solar irradiance on a tilted surface ( $G_t$ ) is:

$$G_{t2} = G_2 \left\{ R_{b2} \left[ 1 - \frac{G_{d2}}{G_2} \right] + \left( \frac{G_{d2}}{G_2} \right) \left[ \frac{1+\cos\beta_2}{2} \right] + \rho_g \left[ \frac{1-\cos\beta_2}{2} \right] \right\} \quad (C8)$$

Where  $R_{b2}$  and  $G_{d2}/G_2$  are the beam radiation tilt factor and characteristic of the sky clearness.

$$R_{b2} = \frac{\cos\theta}{\cos\theta_z} \quad (C9)$$

Expanding and simplifying equation gives

$$G_{t2} = G_2 \left\{ R_{b2} - R_{b2} \left( \frac{G_{d2}}{G_2} \right) + \frac{G_{d2}}{G_2} \left[ \frac{1+\cos\beta_2}{2} \right] + \rho_g \left[ \frac{1-\cos\beta_2}{2} \right] \right\} \quad (C10)$$

$$G_{t2} = G_2 \left\{ R_{b2} + \rho_g \left[ \frac{1-\cos\beta_2}{2} \right] + \left( \frac{G_{d2}}{G_2} \right) \left[ \frac{1+\cos\beta_2}{2} - R_{b2} \right] \right\} \quad (C11)$$

Let

$$a_2 = R_{b2} + \rho_g \left[ \frac{1-\cos\beta_2}{2} \right] \quad (C12)$$

$$b_2 = \left( \frac{1+\cos\beta_2}{2} - R_{b2} \right) \quad (C13)$$

Then Equation for Array 2: AWGA becomes

$$G_2 = \frac{G_{t2}}{a_2 + \left(\frac{G_{d2}}{G_2}\right)b_2} \quad (C14)$$

Array 1 and array 2 give rise to two equations as follows:

$$G_1 = \frac{G_{t1}}{a_1 + \left(\frac{G_{d1}}{G_1}\right)b_1} \quad (C15)$$

$$G_2 = \frac{G_{t2}}{a_2 + \left(\frac{G_{d2}}{G_2}\right)b_2} \quad (C16)$$

These can be solved simultaneously for  $G$ , assuming that  $G_{D1}/G_1$  and  $G_{D2}/G_2$  are the same for the two arrays since the arrays are in proximity to each other and the  $R_{b1}$  and  $R_{b2}$  values vary with tilt ( $\beta$ ) and azimuth ( $\gamma$ ), which are different for the two arrays:

$$G = \frac{G_{t2} - G_{t1} \left(\frac{b_1}{b_2}\right)}{a_1 - a_2 \left(\frac{b_1}{b_2}\right)} \quad (C17)$$

Values of  $G_{t1}$  and  $G_{t2}$  for the two arrays as calculated in Chapter 2 were used in Equation C17, along with calculated values of  $R_{b1}$  and  $R_{b2}$  at each time interval, and assumed values of albedo ( $\rho_g$ ) to calculate  $G$  at a 5-minute intervals for January 1, May 26 and July 2, 2017.

Figures C1, C2 and C3 show the estimated horizontal solar irradiance ( $G$ ) calculated by Equation C17 versus solar irradiance on a tilted surface ( $G_t$ ) plots for both the QEC array and the AWGA array. On the clear and sunny winter day, the estimated horizontal solar irradiance ( $G$ ) values were greater than the estimated irradiance values on the tilted surfaces ( $G_t$ ) at every interval during the analysis period. This result is illogical, given that the sun altitude is less than  $10^\circ$  in the winter, so any southward tilt would increase the solar intensity, making  $G_t$  greater than  $G$ . For the clear and sunny spring and summer

days, the estimated horizontal solar irradiance ( $G$ ) fluctuates below and above the zero mark. In fact, the values for  $G$  are always positive and not negative [1]. The reason why the values for  $G$  are greater than  $G_t$  on the winter day is that the terms in the denominator of Equation C17 are smaller than 1 but larger than 0, resulting in high values. For the spring and summer days the denominator fluctuates from below (negative) to above zero (positive) resulting in  $G$  values that at times are negative and other times are positive. Thus, the method fails to provide a workable algorithm in predicting horizontal solar irradiance ( $G$ ) from back-calculating using the measured solar PV output. Hence, this method was abandoned in favour of that used in Chapter 3.

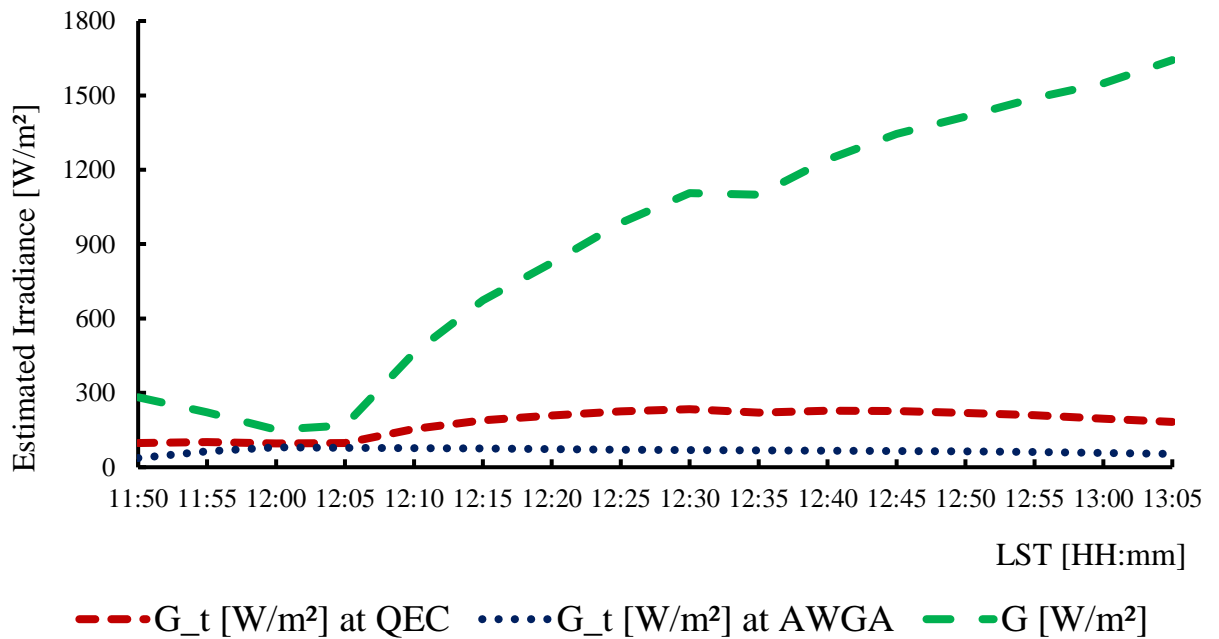


Figure C1 Estimated irradiance for January 1, 2017

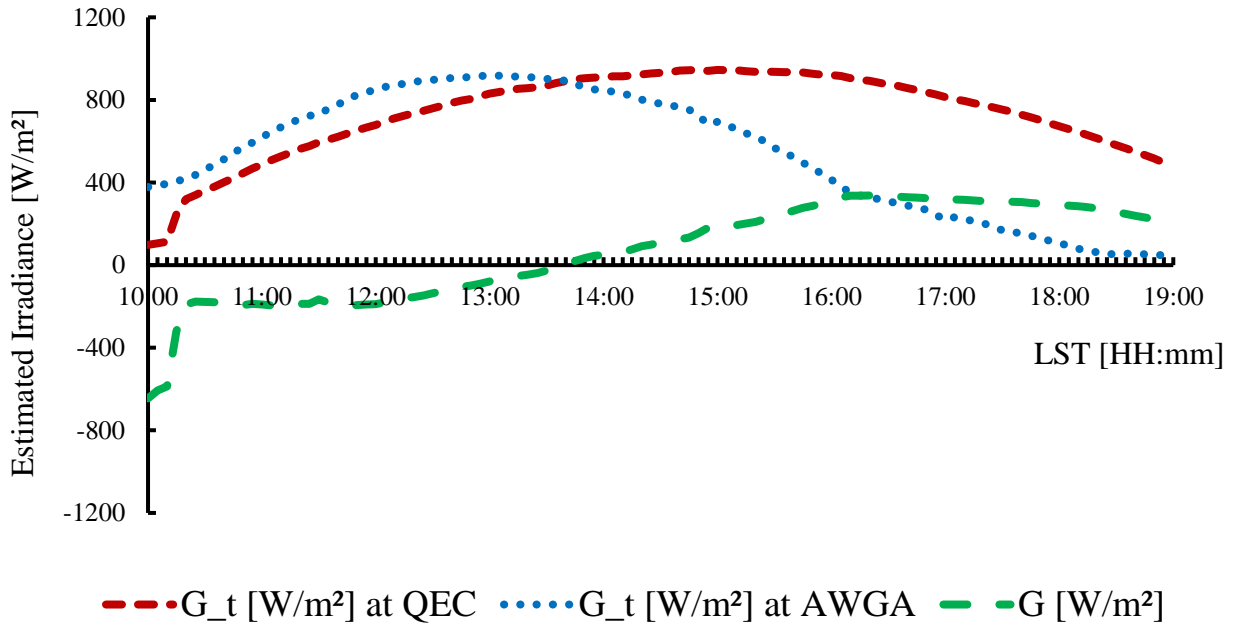


Figure C2 Estimated irradiance for May 26, 2017

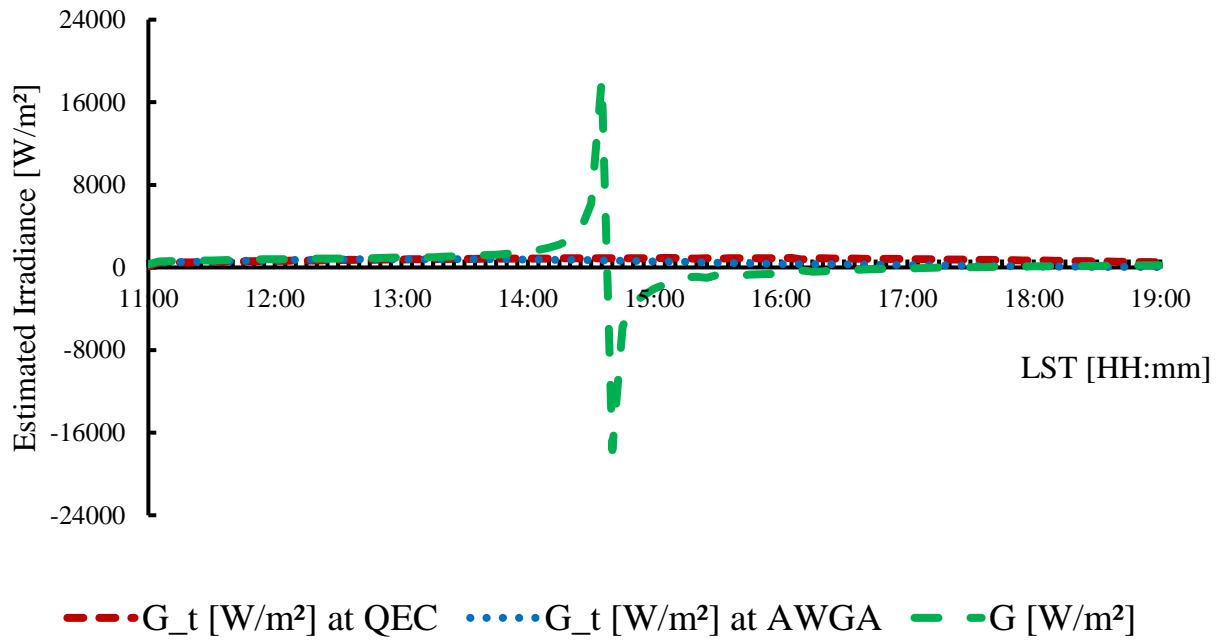


Figure C3 Estimated irradiance for July 2, 2017

## REFERENCES

- [1] J.A. Duffie, W. A. Beckman, W. A., Solar Engineering of Thermal Processes, second ed., John Wiley and Sons, New York, 1980.

## VITA AUCTORIS

NAME: Avinash G. Singh

PLACE OF BIRTH: Georgetown, Guyana

YEAR OF BIRTH: 1982

EDUCATION: University of Guyana, B.Eng. Mechanical  
Engineering, Georgetown, Guyana 2006

University of the West Indies, M.Sc. Engineering  
Management, St. Augustine, Trinidad and Tobago,  
2013

University of Windsor, M.ASc. Mechanical  
Engineering, Windsor, ON, 2020